University of Arkansas, Fayetteville
ScholarWorks@UARK

Theses and Dissertations

8-2012

Fabrication and Characterization of Thinner Solid-State Nanopores

Denis Forbi Tita
University of Arkansas, Fayetteville

Follow this and additional works at: http://scholarworks.uark.edu/etd

 Part of the Biomedical Commons, Health and Medical Physics Commons, and the Nanoscience and Nanotechnology Commons

Recommended Citation
Tita, Denis Forbi, "Fabrication and Characterization of Thinner Solid-State Nanopores" (2012). *Theses and Dissertations*. 510.
http://scholarworks.uark.edu/etd/510

This Thesis is brought to you for free and open access by ScholarWorks@UARK. It has been accepted for inclusion in Theses and Dissertations by an authorized administrator of ScholarWorks@UARK. For more information, please contact scholar@uark.edu, ccmiddle@uark.edu.

Fabrication and Characterization of Thinner Solid-State Nanopores

Fabrication and Characterization of Thinner Solid-State Nanopores

A thesis submitted in partial fulfillment
of the requirements for the degree of
Master of Science in Physics

By

Denis F. Tita
South Dakota State University
Master of Science in Engineering, 2008

August 2012
University of Arkansas

Abstract

Solid State nanopores that are fabricated by the ion beam sculpting process and electron beam drilling have shown great promise as a sensing device for DNA and protein molecules. Even though biological pores such as the α-Haemolysin have been in use for quite some time, the use of solid state Nanopores in single biomolecule detection has been on the rise since the mid 1990s. Solid State nanopores have an advantage over biological pores in that they are more robust, stable, and can be sculpted to any desired size for use in translocation experiments. One of the major challenges in Nanopore fabrication by ion beam sculpting has been limited by the user's ability to control the closure rate of pores in the fabrication process. Another challenge in nanopore sensing is the resolution limitation due to the thickness of the pore. This is because most of the nanopores fabricated by the ion beam sculpting method are often thicker than they should. This thesis will focus on the modification of nanopore fabrication using the ion beam sculpting system at the University of Arkansas by first baking the samples in vacuum under specified temperature conditions. Baking the samples will give the user better control over pore closure. This Thesis will also focus on thinning the sculpted pores by Reactive Ion Etching in an attempt to increase its resolution for single biomecule translocation experiments.

This thesis is approved for recommendation to the

Graduate Council.

Thesis Director:

_____

Dr. Jiali Li

Thesis Committee:

_____

Dr. Surenda Singh

_____

Dr. Hamed Naseem

_____

Dr. Gea Banacloche

Thesis Duplication Release

I hereby authorize the University of Arkansas Libraries to duplicate this thesis when needed for research and/or scholarship

Agreed _____

Denis F. Tita

Refused_____

Denis F. Tita

Acknowledgements

I would like to first thank Dr. Jiali Li for accepting me into her lab and giving me the opportunity to train and work on different projects. Without her guidance and direction in finding solutions to the difficulties that came along this project, this will not have been possible.

My thanks also go to the members of my graduate committee who gave useful suggestions to make this work complete.

I also wish like to extend my special thanks to Dr. Bradley Ledden and Ryan Rollings for introducing and training me in the Nanopore Lab. Their kind and patient approach has been a great motivating factor for pursuing this research.

Table of Contents

Table of Figures

1. Introduction

Since the establishment of the Human Genome project in 1989, billions of dollars have been spent with the primary goal of sequencing and identifying all three billion chemical units in the human genetic instruction set. As recently reported by Genome.gov, DNA Sequencing costs have dramatically dropped over the past 10 years for most large-scale programs. Many different sequencing techniques have been developed over the years with one of them being Single-Molecule DNA Sequencing using Nanopores. In nanopore strand sequencing, a single strand of DNA moves through a narrow pore and the bases are identified as they pass a reading head. Biological Pores such as the α-Haemolysin has been in use for quite some time (Mid 90s) since they are protein transport channels that occur naturally. On the other hand, solid state nanopores are a more recent invention first developed by Li et al at the Harvard Nanopore lab. There are several advantages of solid state nanopores over the biological ones in that they are more robust, stable, and can be sculpted to any desired size for use in experiments. Current nanopore fabrication techniques are promising but there are some challenges in obtaining relatively thin pores that are especially suitable for DNA translocation experiments. The Ion Beam sculpting process used by the Nanopore group at the University of Arkansas is a technique that employs a low energy (1keV-5keV) ion beam to close an existing FIB(100nm) to a smaller nanometer sized hole of about 5-10nm in internal diameter. One of the main challenges with regards to this method has been to control the closure rate of pores in the sculpting process. This is because pores often close too fast there by rendering the closed pore diameter too small, or too large than the desired pore diameter. Other Fabrication techniques such as electron beam irradiation of samples in a transmission electron Microscope have also been employed in order to obtain specified pore diameters. In this technique, the Ion Beam sculpting system is used to close a

nanopore all the way after which a condensed electron beam in a Transmission Electron Microscope is used to drill a nanometer sized hole through a very thin membrane of the closed pore. One other technique employed in the sculpting of a nanopore by the Ion Beam sculpting system is to sputter open an already closed pore under very low temperature conditions in the sculpting chamber. This is done by flowing liquid nitrogen at very low temperatures into the main chamber in order to keep it cool as the sculpting is in progress.

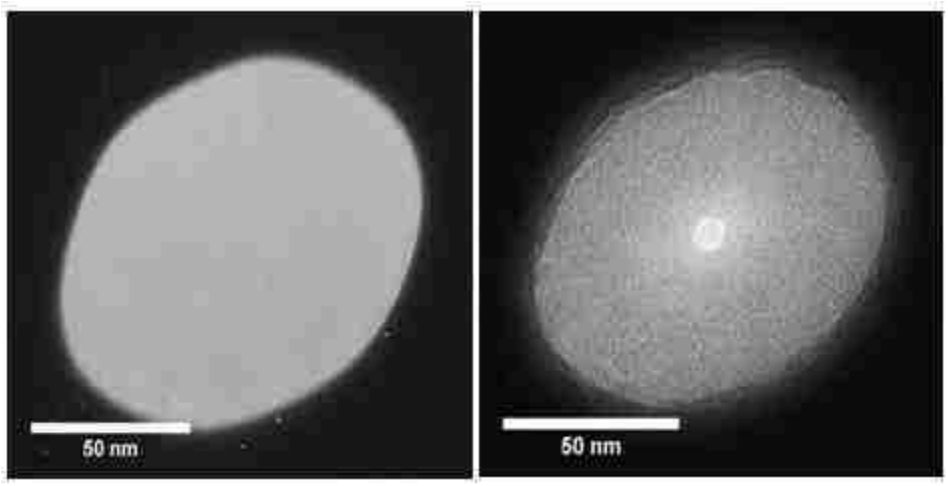

Figure 1: Left is a 100nm sized FIB that is sculpted to about 5nm (Right)

1.1 Motivation

One of the main reasons for baking Nanopores under vacuum conditions prior to closure has been to be able to exert a proper control over their closure rates. Baked pores have been shown to close slower than unbaked pores and this property would give the user the ability to obtain the target pore size or diameter needed. Pores fabricated by the Ion Beam sculpting process would normally have a thickness greater than 14nm and would require thinning them. The main goal for thinning nanopores is to be able to get a better resolution of DNA molecules through them in translocation experiments. A much thicker pore would imply a Low spatial resolution. When the

pore is thinned, the amount of the DNA averaged over the nanopore for a signal will be lowered giving it a high resolution. When a DNA molecule passes through such a pore, it reads about 40 base pairs of DNA segments with lots of details hidden within it. The Nanopore can be thinned by reactive ion etching which is a dry etching method and the principal technique used in the thinning of pores for this research at the High Density electronics center (HiDEC) of the University of Arkansas. Reduction in pore thickness has the benefit in that it will increase the current drop when a DNA molecule is inside a Nanopore and also increase the resolution by increasing the pore's ability to read individual base pairs in the DNA molecule in a translocation process. A DNA translocation experiment using a nanopore can normally be carried out by driving a DNA molecule in an ionic solution through the pore by the application of an electric field. Since a DNA molecule is negatively charged, it will move through the pore toward the anode upon the application of an electric field. Once inside the pore, the DNA reduces the amount of ions that was present in the open pore thus effectively reducing the open pore current. This blockage of ions causes the current to drop and further confirms a translocation has indeed taken place. The current blockade equation further supports the above hypothesis since the change in current is inversely proportional to the thickness of the pore.

$$\Delta I = I_0 - I_{DNA} = V\sigma \frac{A_0}{L_{pore}} - V\sigma \frac{(A_0 - A_{DNA})}{L_{pore}} = V\sigma \frac{A_{DNA}}{L_{pore}}$$

Where ΔI is the overall current drop as the DNA molecule blocks ions inside the pore, I_0 is the open pore current, A_{DNA} is the area of the DNA, V is the applied voltage ,σ is the conductivity of

the solution and L_{pore} is the nanopore thickness.

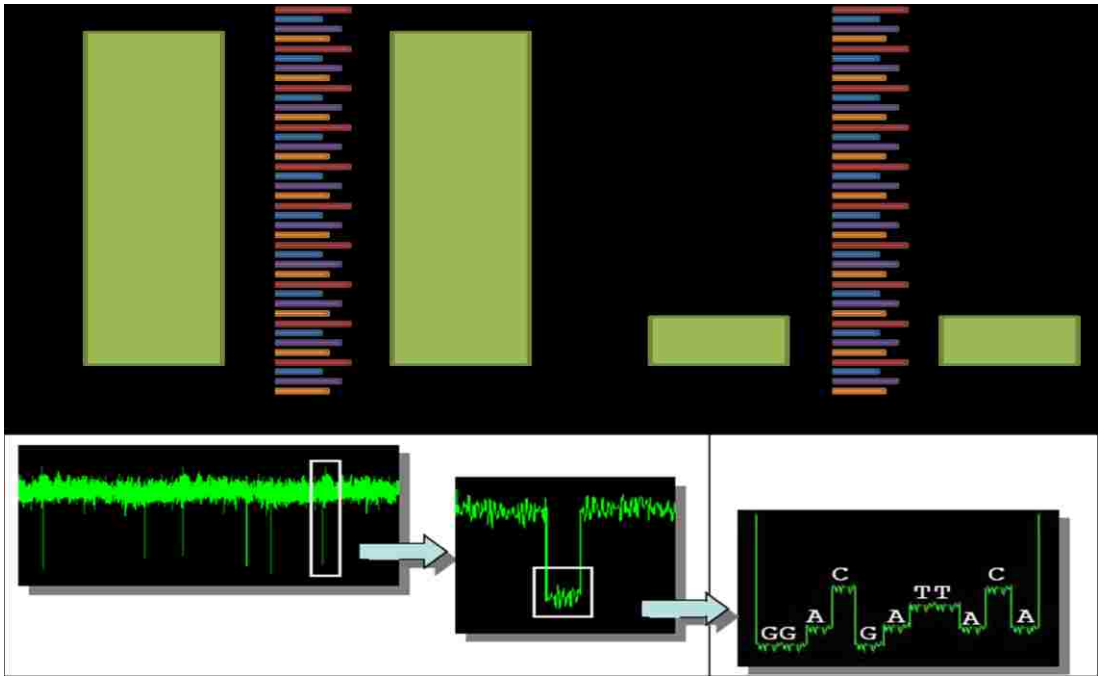

Figure 2: Comparing DNA Translocation through a thick and a thinner Pore

The above figure suggests the current-time graph for the thinner pore has a better resolution than with the thicker pore. When the pore thickness is between 1-2nm, individual base components such as GG A C G ATT AC A can be read thus making sequencing of the DNA molecule possible.

1.2 Organization of this Thesis

This thesis will describe the various techniques employed toward the realization of the above stated goals. The initial wafer preparation techniques such as photolithography, Reactive Ion Etching, Wet KOH Etching, Ion Beam milling will be discussed. Other follow up methods such as Transmission Electron Microscopy imaging of closed pores and the baking of Pores under vacuum conditions in the Ion Beam Sculpting system prior to their closure will also be discussed. The thinning of Nanopores by Reactive Ion Etching as well as a thickness map analysis of the Nanopore geometry will also be examined. This thesis will conclude by examining the results arising from the implementation of the above stated fabrication techniques.

2. Nanopore Fabrication

There are several important steps involved in the preparation of Silicon Nitride wafers before they can be sculpted by the ion beam sculpting technique or drilled by the TEM. A simple silicon wafer is the standard from which all processes begin. A 4X4 inch wafer of about 100mm in diameter with a thickness of about 380 micro meters(μm) is used. This is made of a single silicon crystal with a {100} plane defined on both sides of the wafer

2.1 Low Pressure Chemical vapor Deposition

The initial stage in the fabrication process is done at Cornell University. The process starts with four inch silicon. Silicon nitride coating each with a thickness of about 275nm low stress amorphous Si_3N_4 deposited by the process of Low Chemical Vapor Deposition (LPCVD). Once this process is completed, the wafers are then brought to the Nanopore Lab at the University of Arkansas for further processing.

Figure 3: Side view of Silicon wafer with Si_3N_4 deposited on both sides

2.2 Inspection and Photolithography

The wafers are inspected and cleaned by placing them in a sonicator using arrow shaped holders. They are then sonicated using acetone, Isopropyl alcohol and methanol each for about 15 minutes. After the sonication process, the wafers are rinsed in a Sitek Rinser and carefully dried using Nitrogen. The wafers are then coated by using hexamethyldisiloxane(HMDS) in a Yes oven for about 45 Minutes after which they are then spin coated with a positive photoresist forming a 2.5µm polymer matrix.The wafer is then removed from the spin coater and soft baked

on a Hot plate for time duration of about 120 seconds and at a hot plate temperature of 110^{o}C. Baking ensures the evaporation of any solvents in the resists and also ensures that it glues firmly or tightly to the wafer. After the wafer is cooled, the backside is again coated with resist and baked in exactly the same process as outlined above. Once this process is completed, the wafer is going to appear as shown in the figure below

Figure 4: Wafer with layer of resist coating on both sides

2.3 Alignment and Exposure

The wafer is again inspected for any contamination or defects that may have occurred during the photoresist application. The next step in the fabrication process is to align wafer and mask. A glass chrome mask is carefully aligned on top of the wafer by taping it to three different positions separated by 120^{o} spacing. The mask is aligned to the wafer to ensure that the RIE process that follows, will only etch those portions of the wafer that have been exposed to the UV light. The wafer is then exposed in UV for about 18-20 seconds based on the Exposure time calculations. The chrome portion of the mask blocks light from the mask aligner and prevents the underlying resist from being exposed while all resist underneath the glass portion are exposed.

2.4 Wafer Development

After the wafer is exposed, it develops the pattern of the mask. The wafer, mask and glass plate are then separated, and the wafer is placed in a wafer cassette and immersed in a developer solution and the timer is turned on. After the wafer has been in the developer for about 90 minutes, it is then placed in a dump rinser for about 3 minutes to remove any leftover developer

from the wafer. When the resist is developed, patterns produced will consist of either 3mm by 3mm squares with 560 µm by 560 µm squares inlays or 4mm by 6mm rectangles with 560 µm by 560µm square inlays, as shown in figure 5. The developed wafers are then inspected prior to the reactive ion etch (RIE) step

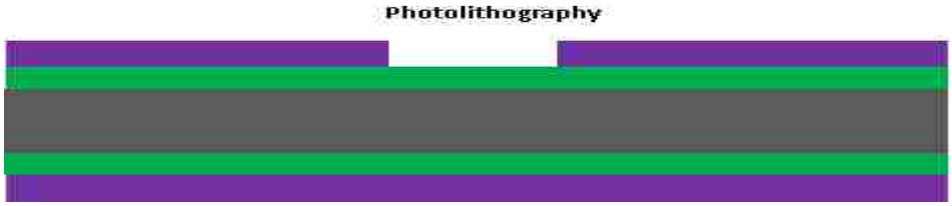

Figure 5: shows a side view of wafer after exposure and Development

2.5 Reactive Ion Etching

The Reactive Ion Etching process (RIE) is an etching technology used in Micro fabrication. It uses chemically reactive plasma to remove material deposited on wafers. This is a dry etching technique as opposed to the wet etching or other known etching methods. The goal of this step is to remove the silicon nitride now exposed according to the mask pattern by photolithography. Removal of the silicon nitride is achieved by generating plasma in the RIE system. The RIE system is composed of parallel plates one of which is capacitively coupled to an RF source, a vacuum chamber and a wafer platter located at the bottom portion of the chamber. The wafer platter or the lower plate is electrically isolated (grounded) from the rest of the chamber. Gas enters through small inlets in the top of the chamber and exits to the vacuum pump system through the bottom. An oscillating electric field RF (13.56 Megahertz) ionizes the gas molecules by stripping them of electrons creating plasma. High-energy ions from the plasma attack the wafer surface and react with it.

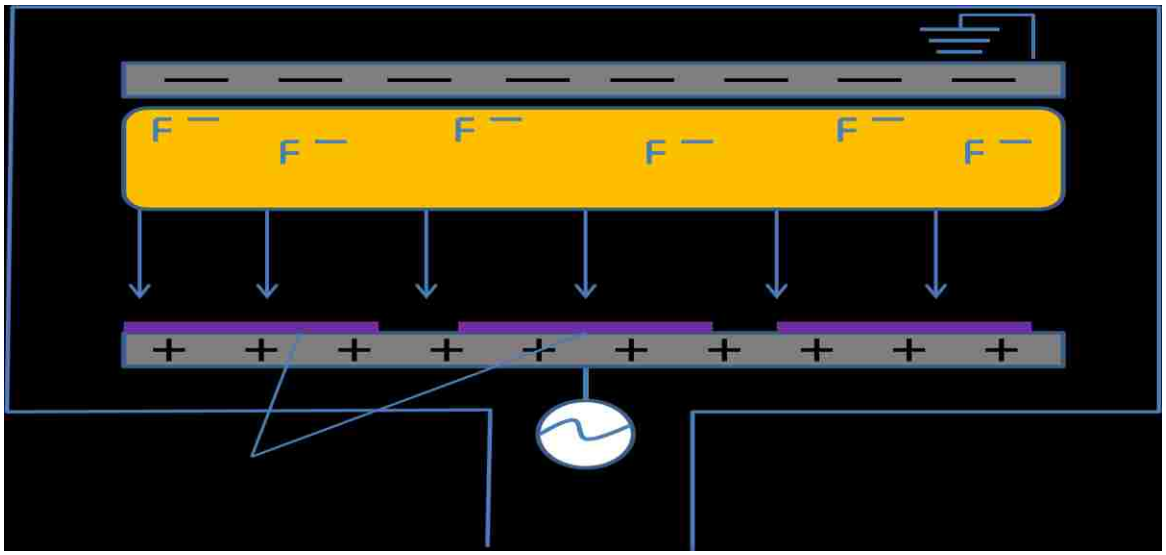

.

Figure 6: (1) and (4) are electrodes that create the electric field (3) meant to accelerate ions (2) towards the surface of the samples (5)

The ions react chemically with the material on the wafer but can also knock off some material by sputtering resulting in etching. Physical etching of the wafer surface is done by ions present in the plasma. Because of the voltage drop between the plasma and each electrode and the resulting electric field, positive ions such as Cl^+ or Ar^+ will strike the wafer surface by knocking off atoms in a more directional manner resulting in Physical etching. The sputtering process tends to etch the wafer in an anisotropic manner thereby narrowing the features of the wafer downward.

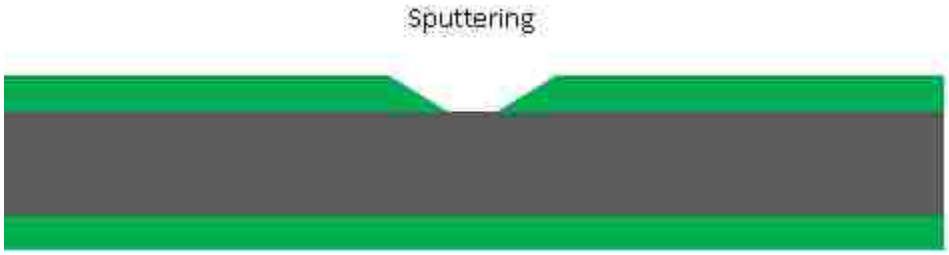

Figure 7: Side view of wafer after the sputtering process in the RIE

Chemical etching of the wafer is commonly done by free radicals and is isotropic. Because of their incomplete bonding structure, free radicals are highly reactive chemical species.

The following chemical reaction is very typical of chemical etching in the recipe

$$e^- + CH_4 \rightarrow CF_3 + F + e^-$$

And $$4F + Si \rightarrow SiF_4$$

Figure 8: Side view of after the chemical etching process

It must be understood that these two etching processes take place simultaneously and a combination of both methods results in straight side walls of the wafer as shown below

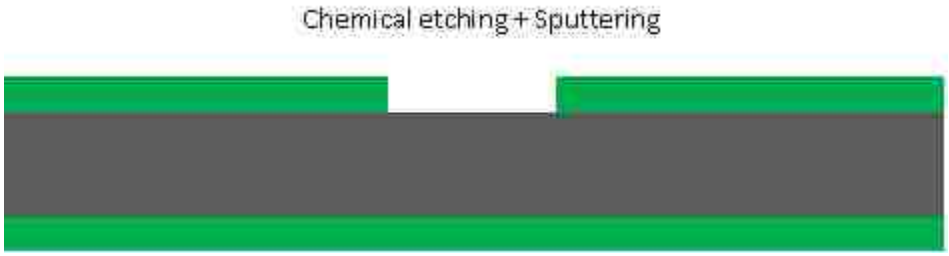

Figure 9: Side view of wafer after the RIE Process is complete

One can see from the above figure that one side of the wafer has the silicon nitride removed in the exact pattern of the mask. Before beginning the RIE process, the RIE chamber must be cleaned. Cleaning the chamber will also help get rid of any impurities that might have been left over in a previous etching process. Cleaning will also help warm-up and stabilize the system.

When the system is stable prior to etching, it can help avoid early etching and wrong etch rate values. The table below gives the cleaning recipe for the RIE

STEP	TIME(MIN)	PRESSURE
1	0:10	0.002Torr
2	0:30	40mTorr
3	5:00	40mTorr
4	0:30	600mTorr
5	5:00	500mTorr
6	1:00	10mTorr
7	0:15	0.001mTorr

Table1: Recipe used to clean RIE Chamber with Oxygen as the Plasma

After the cleaning process is complete, the chamber is vented and the lid opened. The Wafer can be loaded into the main chamber either manually or by an automated process from the Loadlock. In the automated process, the wafers are placed in a vacuum sealed load lock that contains a wafer loading tray. A command is initiated by pressing the appropriate button. The tray then transfers the wafer into the RIE plasma chamber. Once the wafer is in the chamber, the appropriate program is then loaded and run to etch the wafer. The manual process is done by raising chamber lid and bracing with a PVC pipe. An Aluminum shield in the chamber is then removed and replaced by an Ardel shield with a clean 5in dummy wafer at the center. The wafer to be etched is placed in the chamber with the side to be etched facing up on the center of the dummy wafer. Close lid and pump down system until sufficient vacuum has been established. System pressure can be read on the monitor as it pumps down. It takes about 15 minutes to complete the pump down process. Once system pump down is complete, the Etching recipe is then loaded and run to etch the sample. The recipe used to etch the sample is composed of 15 sccm of Ar, 15sccm of CH_4, 2 sccm of O_2 and an RIE power rating of 100W.

STEP	TIME(MIN)	PRESSURE	CH_4	Ar	SF_6	O_2	POWER
1	0:10	0.01mTorr	0	0	0	0	0
2	0:30	20mTorr	15	15	0	2	0
3	VARIES	20mTorr	15	15	0	2	100W
4	1:00	10mTorr	0	0	0	0	0
5	1:00	10mTorr	0	0	0	0	0
6	0:30	7mTorr	0	0	0	0	0

Table2: Recipe used to Etch Wafer

As can be seen from the recipe, the first two steps control the flow of gas into the system while the etching actually occurs in the third step. The etching time can be adjusted as needed and would normally depend on the etch rate calculation preferably from test samples of the same wafer. Using test samples from the same wafer set will help minimize etch-rate errors that might have resulted from having to use a different wafer set of samples. The formula for calculating the etch time is as given

$$ETCH...RATE = \frac{THICKNESS..REMOVED}{TIME}$$

Once the etching process is completed, an alarm will sound or a report will be displayed on the computer screen to indicate the end of the process. The main chamber is then vented and the wafer unloaded. The wafer is then taken again to the nanospec to ascertain the success of the etching. The nanospec thickness value would normally serve as a verification as to whether all the silicon nitride in the trench has been removed. If the silicon nitride is not completely removed, then the etch-rate and RIE parameters would be adjusted as necessary and the process repeated. The RIE system must be shut down once you're done using it. Remove the Ardel electrode and replace it with the Aluminum electrode. Close the lid and pump down the system. Once the pump down is complete, run chamber clean to clean the chamber, fill process log , check gasses and their pressures before leaving the RIE. Once the RIE step has been completed,

the wafer is then brought back from the HiDEC Center to the Nanopore lab for the next processing step which is Wet KOH etching.

2.5.1 Effects of Temperature and Pressure on the RIE

Increasing the pressure causes more gas-phase collisions to occur, decreasing the directionality of the etching. Plasma densities decrease at a higher pressure resulting in a decrease in Ion energy and sputter yield. This implies that the Etch rate decreases with an increase in Pressure. The effect of increasing the pressure on the ion-flux is less clear cut and different systems show different relationships. Usually the temperature of the etch system; including the wafer is not intentionally raised during the etching. The plasma supplies the energy for the etch process and heating the gas or wafer would not significantly increase the etch rate or improve the process.

2.5.2 Effects of RF Power and Gas Composition on the RIE

Increasing the RF power increases the plasma density and the self bias voltage. This gives rise to an increase in the Ion energy and the sputtering yield which results in a higher physical component of etching and an increase in the Etching-rate**.** The RF power was varied from 50W to 100W and the corresponding etch-rate values were determined as depicted in figure10.

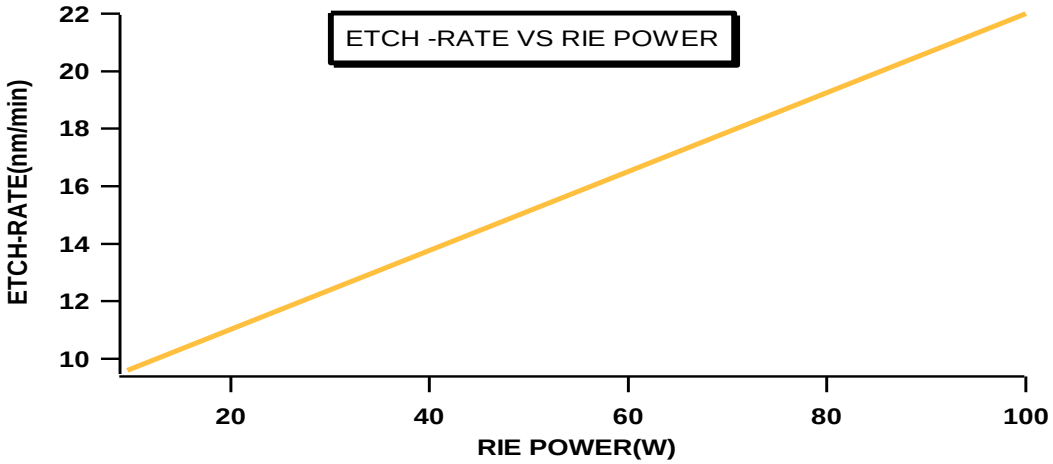

Figure 10: Etch-Rate Vs RIE Power

The flow rate often have a minor effect on the etch rate. Increasing the flow rate will initially increase the etch rate by producing more reactive species. But the actual supply of reactant species depends on the balance between generation and loss of species in the plasma, and a steady state is reached where the etch rate is independent of gas flow.

2.6 Wet Chemical Etching

This part of the fabrication is done by submerging the wafers in a solution of specially prepared 30 wt KOH at 90^{o}C for about 4hours. Stir and monitor wafer every 20 minutes until you see clean squares. During this process any remaining photoresist will be etched from the Si_3N_4 surface. The KOH solution also etches the (100) face of the exposed silicon along the [111] plane thus creating a pyramidal shape inside the silicon at an angle of 54.74 degrees with respect to the surface. After the wet etching process is over, the wafer would have been etched through one layer of Si_3N_4 and through the silicon crystal layer leaving a freestanding membrane of Si_3N_4 on the other side

Figure 11: KOH etching with a free standing membrane of Si_3N_4

2.7 Focused Ion Beam Milling

The Focused Ion beam milling of the free standing membrane is done at Harvard University. In the FIB milling process, the user aims for an FIB diameter mostly in the range from 80nm-100nm because it gives a margin of error for larger and smaller FIB holes that can be closed

from 100nm or less to a nanopore. The final step is to image and measure the diameter of the individual FIBs using a transmission electron microscope.

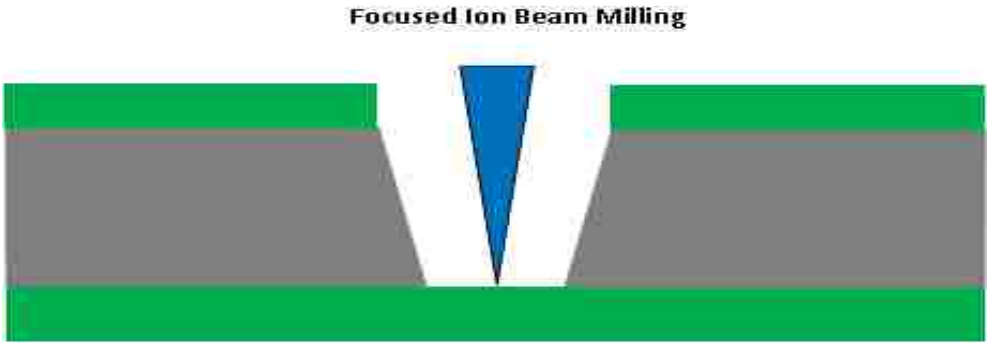

Figure12: Focused Ion Beam Milling

3. Steps Involved in Nanopore Scupting

There are four primary techniques available for the fabrication of solid-state nanopores in thin Si_3N_4, SiO_2, Al_2O_3 or polymer membranes. These include surface tension driven oxide reflow, ion beam sculpting, track-etch method and electron beam based decompositional sputtering. The principal method of interest used in this experiment is the Ion Beam Sculpting technique that uses energetic noble gas ions to bombard the surface of a silicon nitride membrane around the FIB hole. These heavy ions will knock off atoms around the FIB and as a result of a concentration gradient, the more energetic surface adatoms will migrate towards the FIB hole leading to the formation of a Nanopore.

3.1 Sample Alignment and Placement in System

Before beginning the sculpting process, the system must be powered up and the deflection plates and lenses set to the appropriate voltages. The neon gas line must then be purged to ensure it is free from contaminations. The sample which could either be a 3X3mm or a 4X6mm chip is placed in a fitting of the sample holder and held tight by means of spring fingers on top of the sample holder. This keeps the sample from falling off when placed inside the main chamber. The sample holder also consists of a thermal resistive device (RTD) attached to it to help keep track of the temperature of the sample during the sputtering process inside the main chamber. The sample is then aligned by placing the holder on the mock stage of an inverted microscope. The mock stage is a replica of the one on which the sample sits when inserted into the main chamber. The alignment is done by manually tightening the holder with a screw on the mock stage on the Alignment stage of the microscope. The alignment is completed by centering the cross hairs of the microscope glass lens on the 30µmX30µm free standing membrane. The sample is then placed in the load lock and pumped down to about 10^{-7}mbar. The load lock system is pumped by

a Pfeiffer TMU 261 turbomolecular pump backed by a Pfeiffer DUO 005M rotary vain pump. The turbo pump is separated from the load lock by a gate valve so the load lock can be brought to atmospheric pressure without shutting down the turbo pump. Pumping down from atmospheric pressure, the load lock is first rough pumped with a Varian SH-100 dry scroll pump to about 10^{-2}mbar before the gate valve is opened and the turbo pump is allowed to pump down to a high vacuum pressure of 10^{-7}mbar. The pump down process normally takes about 30 to 45minutes and may be shorter depending on how well evacuated the system is.

Figure 13: Alignment microscope used in aligning the sample

A Pfeiffer TPR 265 pirani gauge monitors the pressure in the vacuum line between the scroll pump and the load lock. The load lock is also equipped with a magnetic transporter to slide the sample holder into the main chamber. The flange across from the load lock contains a pressure gauge, a heating element, and a quadrupole mass spectrometer. The pressure gauge is a Pfeiffer PBR 260 hot cathode gauge. This gauge measures the pressure of the main chamber.

Once the pump down process is complete, the sample is then moved into the main chamber by use of the magnetic transporter. The sample sits on a sample holder in the main chamber and it is from this position that it sculpted by ion bombardment.

3.2 The Vacuum system Overview

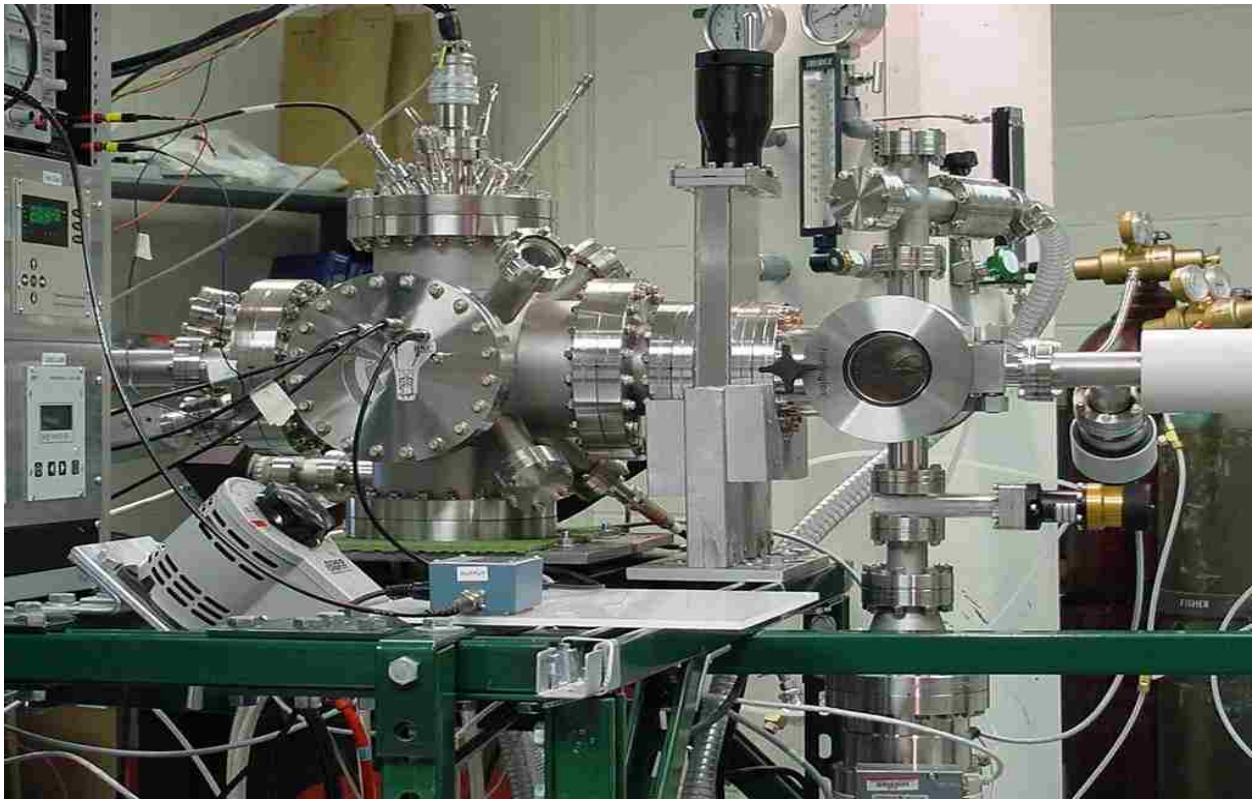

Figure 14: The Feedback controlled Ion Beam Sculpting System at the U of A

The main components of the system are housed in a chamber which is kept at about 10^{-9}mbar vacuum. The Chamber is a six way cross with 8 inches flanges from the MDC vacuum products Corporation. There is a Turbo Molecular pump at the bottom of the chamber that is responsible for creating the vacuum. It is backed by a Varian DS102 dual stage rotary vane pump. At the top flange of the chamber, there are electrical and liquid nitrogen feed-throughs and supports for the sample stage and ion lens components. The sculpting chamber is also equipped with a load lock to prevent venting the entire chamber from one sample to the next. Thus it is more convenient and safe to vent the load lock while the main chamber remains pumped down. This is possible since the load lock is separated from the main chamber by a gate valve so the load lock can be brought to atmospheric pressure without venting the main chamber.

3.3 The Nanopore Sculpting Process

Once the sample is securely placed in the main chamber, the ion gun pressure is set to $(2 \pm 0.2) x 10^{-6} mbar$. This can be adjusted by turning the leak valve slowly. The channeltron voltage is set to 2.20keV and the einzel lens to 2.35keV ion acceleration. These numbers represent the settings that gave the most counts of ions passing through the sample during the beam alignment process. The beam switch voltage control is powered on by setting the control state as low. Low implies the ion beam is deflected away from the sample. Power on the ion gun filament and wait three minutes before setting the emission current. At this point, a check must be done to ensure the ion beam is not hitting the sample. This can be verified by checking that there are no counts on the counter. The High voltage button on the ION GUN supply is then powered on to accelerate the ion beam. The current measured in the keithley picometer initially goes up so a wait time must be observed for the current drop to stabilize. After the current and the beam have stabilized, the counter is restarted to ensure it is properly initialized by LabVIEW$^{TM.}$ The electron gun power supply is turned on. Run the LabVIEW^{TM} counting program. This program initiates the digital counter and the number of counts recorded by the channeltron. The number of dark counts should be somewhere between 0-3counts/500ms. Flip the control stage as Ext to allow the ion beam to hit the sample. The LabVIEW^{TM} program will record the ion counts. The ion bombardment with 3KeV neon ions is achieved by means of a VG Microtech EX05 differential pump ion gun capable of generating an Ion beam of energy 0.5 to 6.0keV with a minimum diameter of 120µm depending on the gun parameter adjustments. As the ions strike the surface around the nanopore, it produces a sputtering effect that generates surface adatoms. The more energetic adatoms will diffuse as a result of a concentration gradient around the pore by forming a thin layer of material that result in its closure. The Ion Beam sculpting

apparatus not only uses ions as a nanopore sculpting tool, but also uses the ions transmitted through the pore as a measure of the area or diameter of the pore under fabrication. The initial ion counts are large and gradually reduce as the pore closes indicating a smaller pore area. Ions transmitted through the pore, are refocused by the einzel lens to the energy analyzer. The Energy analyzer plates are curved at an angle of 60° and are kept at voltages of ± 280V for 3keV incident ions. The angle and voltages only allow the ions with the proper energy to enter the Channeltron to be counted. The einzel lens is composed of three elements, of which, the first and third are held at the same voltage. The outer two lens parts are grounded to help act as a shield for the energy analyzer plates and the Channeltron thus blocking stray ions in the sculpting chamber from contaminating the ion beam count. The second lens element is held at 2.35kV for 3keV ions. After the einzel lens refocuses the ion beam, the ions travel through a post-einzel deflection plates. The single Ion detector measures the ions and converts every detected ion into an electronic pulse. The electronic pulses are then counted by a digital counter and read by a LabVIEW™ program which also controls the voltage that will deflect the ion beam away from the sample. The sculpting process is thus terminated when the required number of counts for pore closure is attained. The constant bombardment of the free standing silicon nitride membrane with ions from the ion gun will cause a build of positive ions on the sample since it is an insulator. This will cause the undesirable effect of repulsion of the incoming ions. To combat this problem, a Kimball Physics FRA-2x1-1 electron gun is used to saturate the surface with electrons to neutralize the positive charges. A diagrammatic overview of this process is shown in figure 14

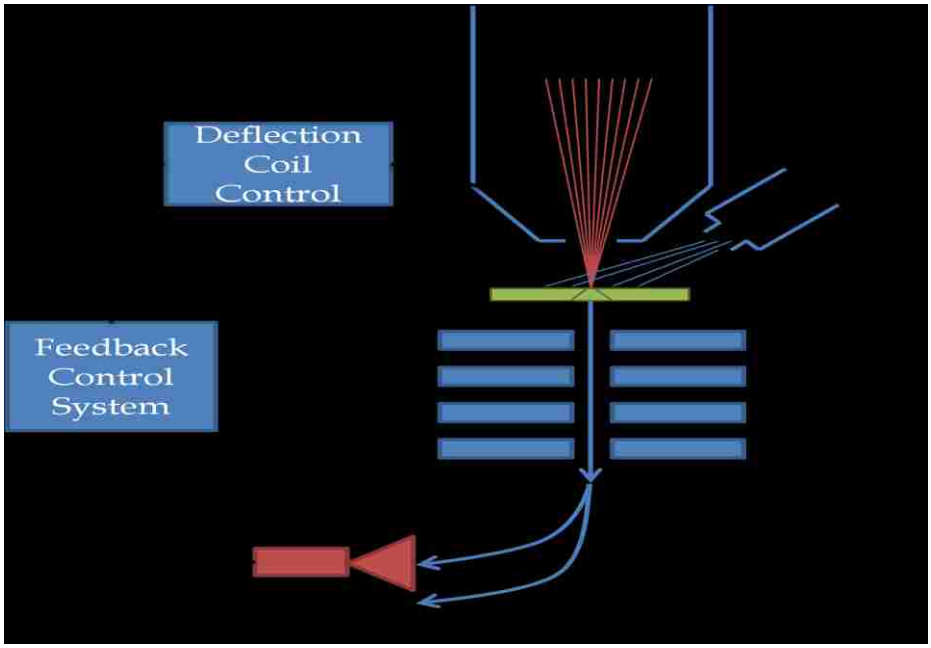

Figure 15: Schematic of the feedback control tool.

3.4 Closing Area and Diameter of a Sculpted Nanopore

In order to determine the final diameter or area of the fabricated pore, one must first find the diameter of the FIB and the flux of the incident beam. The diameter of the FIB can be found from the equation

$\frac{d(mm)*(1x10^6)}{M} = W(mm)$, where d is the diameter of FIB in millimeters, M= magnification of microscope and W is the width of the FIB in millimeters. The magnification most frequently used is 250,000 times but other magnifications have been used as well. The area of the FIB is calculated by assuming it to be an ellipse with a major and a semi minor axis. The FIB diameter can also be measured along both axis using Image J and the actual diameter is the geometric mean of the two values. The area is calculated from the following formula $A_{FIB} = \frac{\pi}{4}(d_1)$ X (d_2).Where d_1 = diameter across major axis, d_2 = diameter across minor axis and A_{FIB} = Area of FIB. The FIB area is then used to calculate the initial area of the pore

from the given flux measurements. The flux $\Phi_1 = \frac{BC}{A_{FIB}}$, Where Φ_1 is the initial flux, BC= beginning counts and A_{FIB} = area of FIB. Once the sculpted nanopore diameter or area has been decided upon, a direct proportionality relation can be used to determine the number of counts that will give the desired pore area or diameter as can be shown from the following calculations. If the Flux through the Nanopore is given by Φ_2 = (End counts)/ (A_{PORE}), then we can determine the closing pore area from the end counts by constancy of the flux since $\Phi_1 = \Phi_2$. $Endcounts = A_{pore} * \frac{BC}{A_{FIB}}$. We can thus calculate the number of counts that gives the desired pore area and hence the diameter of the fabricated pore.

3.5 Post Sculpting Analysis of Pore

Once the pore sculpting process is complete, the Sample is then removed from the sculpting system for further TEM imaging to determine if the desired pore diameter was achieved or if there were other parameters or defects that may have occurred as a result of the sculpting process. Precision or exactness of pore size is always difficult since some pores close too fast and control is often very difficult. There could be many causes such as dirt in the pore, water in the main chamber or some other contamination which will normally require a separate analysis such as X-ray photoelectron Spectroscopy (XPS) or electron energy loss spectroscopy (EELS) to determine the elemental composition of the material or using the residual gas analyzer to track vacuum contamination of the Ion beam sculpting system. Other attempts to control the closure rate of nanopores such as baking and thermal annealing have been used to control pore closure rate to some extent. It has been shown that baked pores would close slower than those not baked though this is not generally true for all pores examined in this study. In order to bake pores under vacuum conditions, the system must be calibrated. The motivation for calibrating the system is to

be able to keep track of the baking temperature of pores before they are closed. This is because temperature plays a vital role in the closure rate of pores. The next section describes the system calibration process.

3.6 Temperature Calibration

Before the baking of pores began, a temperature calibration of the system was performed in order to be able monitor sample temperature at all stages of the baking process. A thermal resistive device was glued to the sample holder by using Epothek – Tek glue confirmable to vacuum conditions as shown in figure 16.

RTDs uses electrical resistance and require a power source to operate. The resistance ideally varies linearly with temperature. They produce a positive change in resistance for a positive change in temperature as in the equation below.

$$R_T = R_0 + R_0\alpha\left[T - \delta - \left(\frac{T}{100} - 1\right)\left(\frac{T}{100}\right) - \beta\left(\frac{T}{100} - 1\right)\left(\frac{T}{100}\right)^3\right]$$

R_T = Resistance at temperature T, R_0 = Resistance at 0^0C

∂ = 1.49(typical for platinum), $\propto$= temperature at T = 0^o

β = 0 for T> 0 and 0.11 for T< 0

Only the linear part of the above equation has been assumed for all calculations in this experiment since higher powers of T are very small and as such can be neglected.

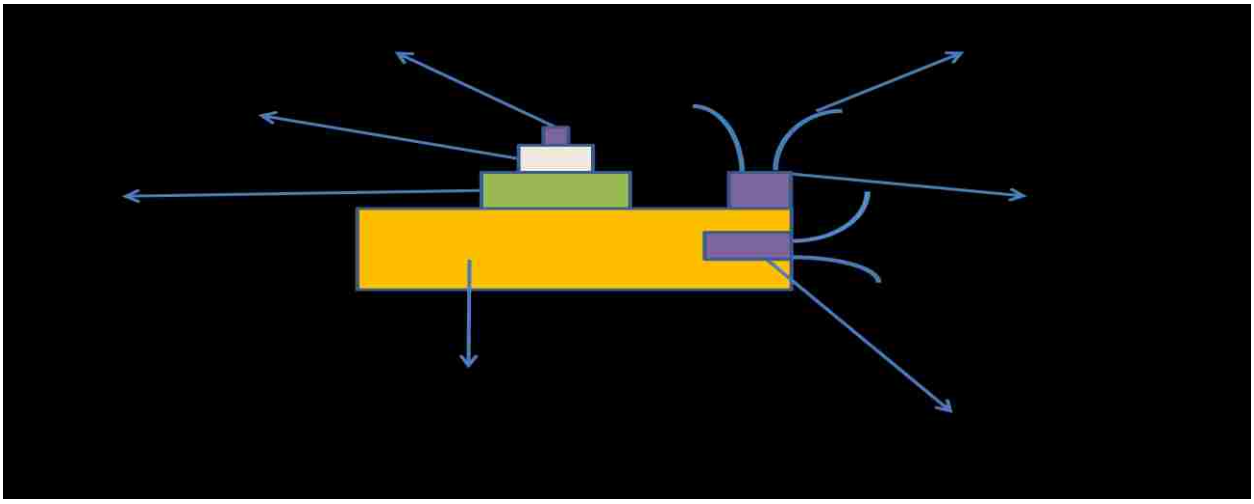

Figure 16: Overview of RTD attached to sample Holder by Glue

The sample holder was then placed in the load lock and a connection between the RTD, and the Micro Controller device (Calibrated for 100ohms at zero degrees) was established. After pumping down the load lock to 10^{-7}mbar, the light bulb was turned on at a variable auto transformer rating of 10%. Temperature values were then read off every 10-15 minutes from the micro controller device until a steady state condition was reached. Since the sample (chip) is glued to the RTD, the RTD temperature is generally assumed to be the same with that of the sample at any given time in the baking process. The sample is baked by turning on the light bulb in the load lock and keeping the Variac transformer power rating at 10%. As the brightness of the bulb is increased, the heat from the bulb is then used to heat the sample and the RTD. The change in temperature for the RTD device was then recorded for different trials and the result for the first 10 minutes is shown in table 3. Figure 17 shows a graph of Average temperature Vs time for different trials as the sample was being baked in the load lock. The temperature steadily increases until it reaches constant value after which a steady state is reached. The temperature of the sample at any specified time can be calculated once the slope of the graph is determined. The Micro controller reading will give slightly higher than expected values and as such a calibration

of the RTD outside of the load lock will help find a correction factor for the actual Sample/RTD temperature.

Power	Time(Mins)	Time(seconds)	Average temperature
10%	0	0	37.86
10%	1	60	51.86
10%	2	120	66.36
10%	3	180	80.12
10%	4	240	91.64
10%	5	300	104.46
10%	6	360	116.62
10%	7	420	128.06
10%	8	480	138.98
10%	9	540	149.18
10%	10	600	159

Table 3: Temperature values with RTD in Loadlock

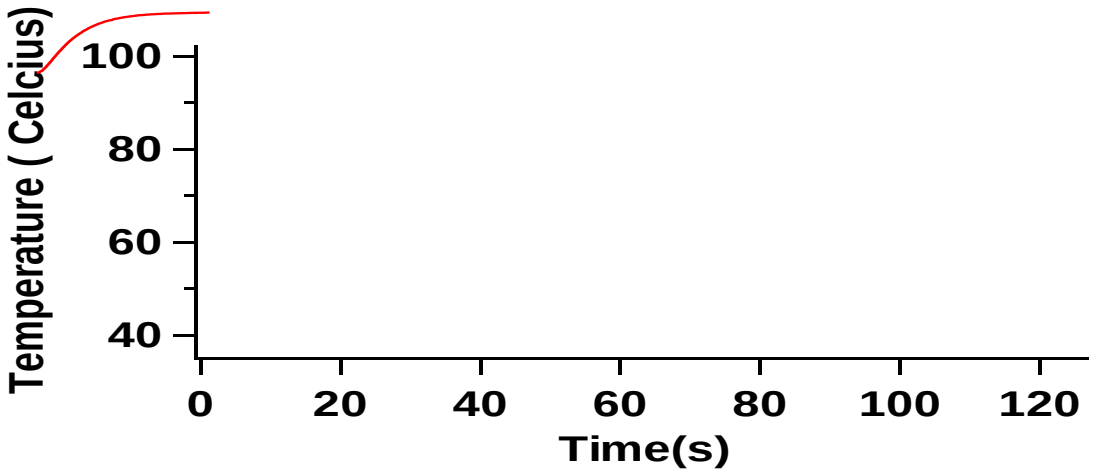

Figure 17: Average temperature Vs Time for sample in load lock

The Idea of a second calibration outside of the load lock is to correct for any temperature errors that may have resulted from the previous calibration. The thermal resistive device (RTD) together with the sample holder was then taken out of the load lock and a connection between RTD and the micro controller device established by means of steel wires. At a room temperature

of 25^0C, the initial RTD temperature at the micro-controller read 38^oC. This reading from the controller is clearly above room temperature suggesting a correction to the controller reading. The RTD was next placed in ice water with a glass thermometer inside. The glass thermometer gave a reading of 2^oC while the Micro controller gave a reading of 14.1^oC. It is to be assumed that the glass thermometer reading when the RTD is in the ice water is the correct reading since the glass thermometer and RTD are both in the water. There was a wait time of about ten minutes for the controller to reach room temperature. The above process was then repeated with boiling water at 100^oC and at other temperatures values with the following results and graph.

Glass Thermoter temperature	RTD Temperature
2	14.1
24	36.4
25	38
87.2	101.9
88.5	103.3
92.1	106.6
96.8	110.2
97.4	110.5
100	111.3

Table 4

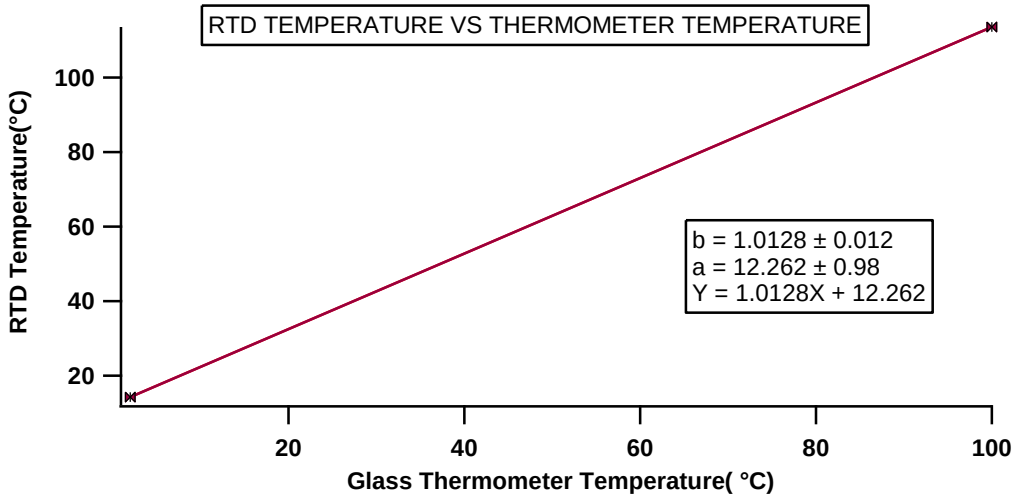

Figure 18: RTD Temperature Vs Glass Thermometer Temperature

The linearity of the above figure is in excellent agreement to what was expected since the resistance of RTDs varies linearly with temperature. The above graph also gives us an intercept value a = 12.262±0.98 which is the error for this experiment. This therefore suggests subtracting 12.262±0.98 from every temperature reading on the micro-controller device to get the actual sample temperature when baking pores in the load lock.

3.7 Temperature control in the Main Chamber

In order to investigate the effects of temperature on the closure rate of pores, a steady temperature needs to be established on the sample. Pores tend to close much faster at higher than at lower temperatures. When the temperature is too low, pores tend to open up when they are bombarded by a stream of ions. This suggests keeping the temperature of the main chamber controlled. The temperature of the sample can be directly controlled by using the Micro-Mega controller device which is incorporated in the Ion Beam Sculpting system. A complete circuit description of the control mechanism is as shown below.

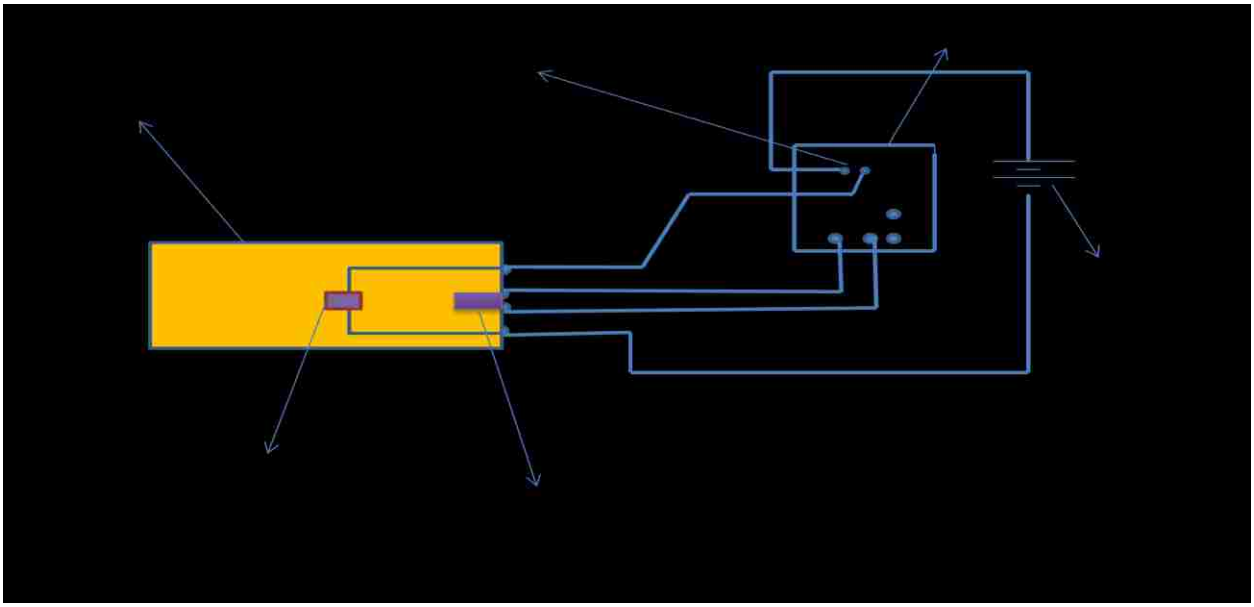

Figure 19: Temperature Control Circuit for Sculpting System

The RTD on the sample holder is connected to two of the conducting spring fingers while the 1watt resistor heater is connected to the other two spring fingers in the center. When the sample holder is placed in the main chamber, a connection between the RTD, the heating element and the Micro-controller device is established. The DC power supply connects both the internal resistor of the holder and the solid state relay located inside the controller. When the controller accepts a temperature signal from the RTD as an input; it compares this temperature value to the set point value. If it is less than the set point value(normally room temperature), the controller turns on the relay which connects the power to the heater to heat up the sample to the desired temperature. If the RTD temperature is higher than the set point value, the controller output (Relay) turns off the power supply to the internal resistance thus allowing the sample to return to the set point temperature. The on/off process of the controller thus helps to keep the sample at a controlled temperature

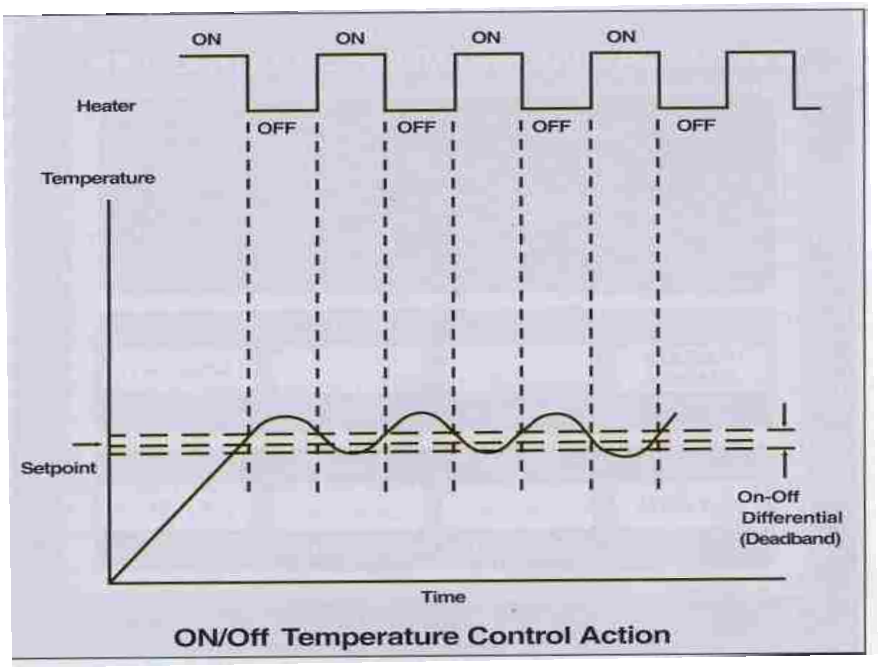

Figure 20: On/Off Temperature Control Action of the Micro-Mega Device

3.8 Baked and unbaked Pores

The motivation for the baking of Pores prior to closure is that baked pores have been shown in general to close much slower than unbaked pores. One other reason has been to be able to control their closure rate. This is generally not true in all cases as some baked pores have been shown to close much faster than predicted. There are still lots of unknowns at the nano-scale as to why this is so. There have been some suggestions that unclean pores would not close slower even if they are baked because of contaminants at the surface of the material. While this may be true in some cases, it has never been substantiated by solid experimentation or any known spectroscopic methods such as XPS.

TEM images of Samples were taken to determine FIB diameter before the baking procedure was performed. All pores in this study were backed at a 10% power rating for 10 minutes. According to the calibration data previously obtained, this will correspond to a sample temperature of 122^0C after all correction factors are considered.Figure21 shows the TEM images of a pore before and after baking for 10 minutes at 10% power rating of the transformer up to a temperature of about 122^oC.

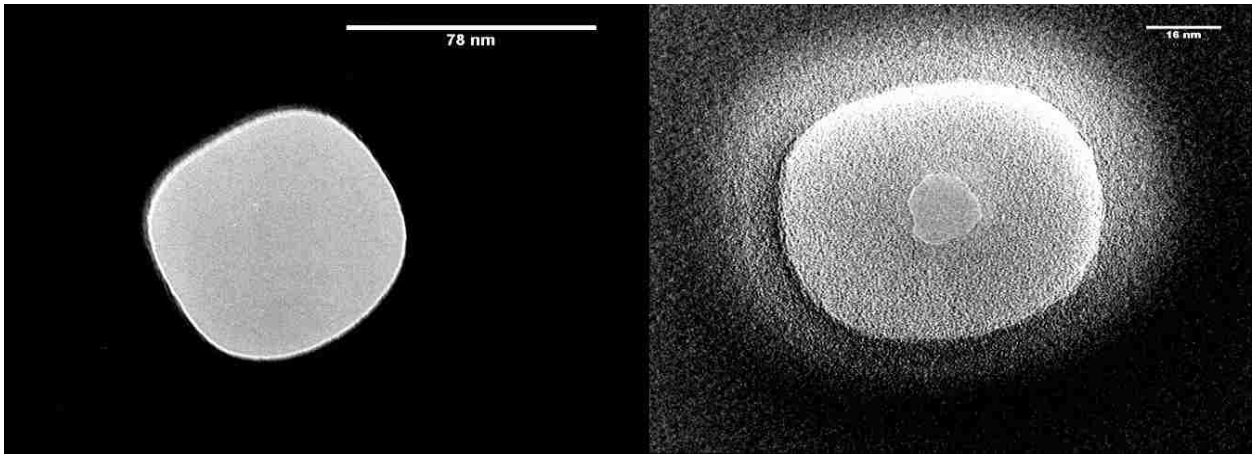

Figure 21: Left is the FIB picture before baking. Right is the Pore image after baking and closure

Graphs for the closure rate of baked pores and pores that were not baked have been plotted in figure 22.

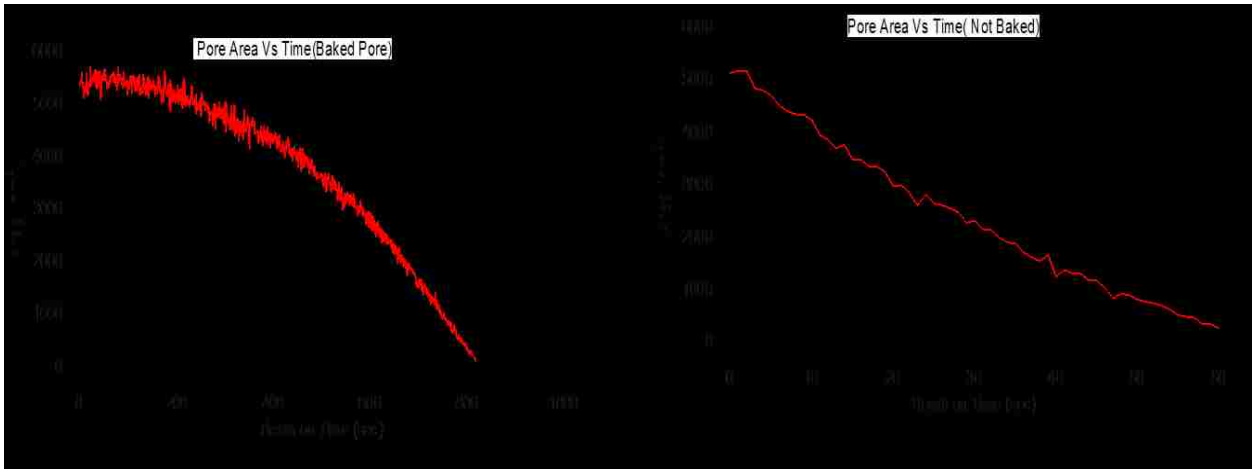

Figure 22: Closure time for baked (Left) and unbaked pores (Right)

As can be seen from the graphs, the baked pore took a relatively longer time to close than the pore which was not baked. The graph for the baked pore is somewhat concave suggesting a slower closure rate initially and a faster rate toward the end. The overall closure time took about 820s. The Graph for the closure rate for the unbaked pore is almost entirely linear with an overall closing time of about 50s. The result from the above graphs suggests that the pore closure could more easily be controlled when it was baked prior to the closing process. The above study was extended by examining the closing time for several baked and unbaked pores and a Histogram to compare their closing time is shown in figure 23.

As can be seen from the Histogram of baked pores, there is a wide spread in time for the number of pores baked at 122^0C for a 10% power rating of the sculpting experiment. It also shows some baked pores took as long as 3000s to close. The Histogram for the unbaked pores shows that all the pores had closed by the time we get to 1500s. From the Histograms below, it can be concluded that when pores are baked, they closed much slower than if they are not.

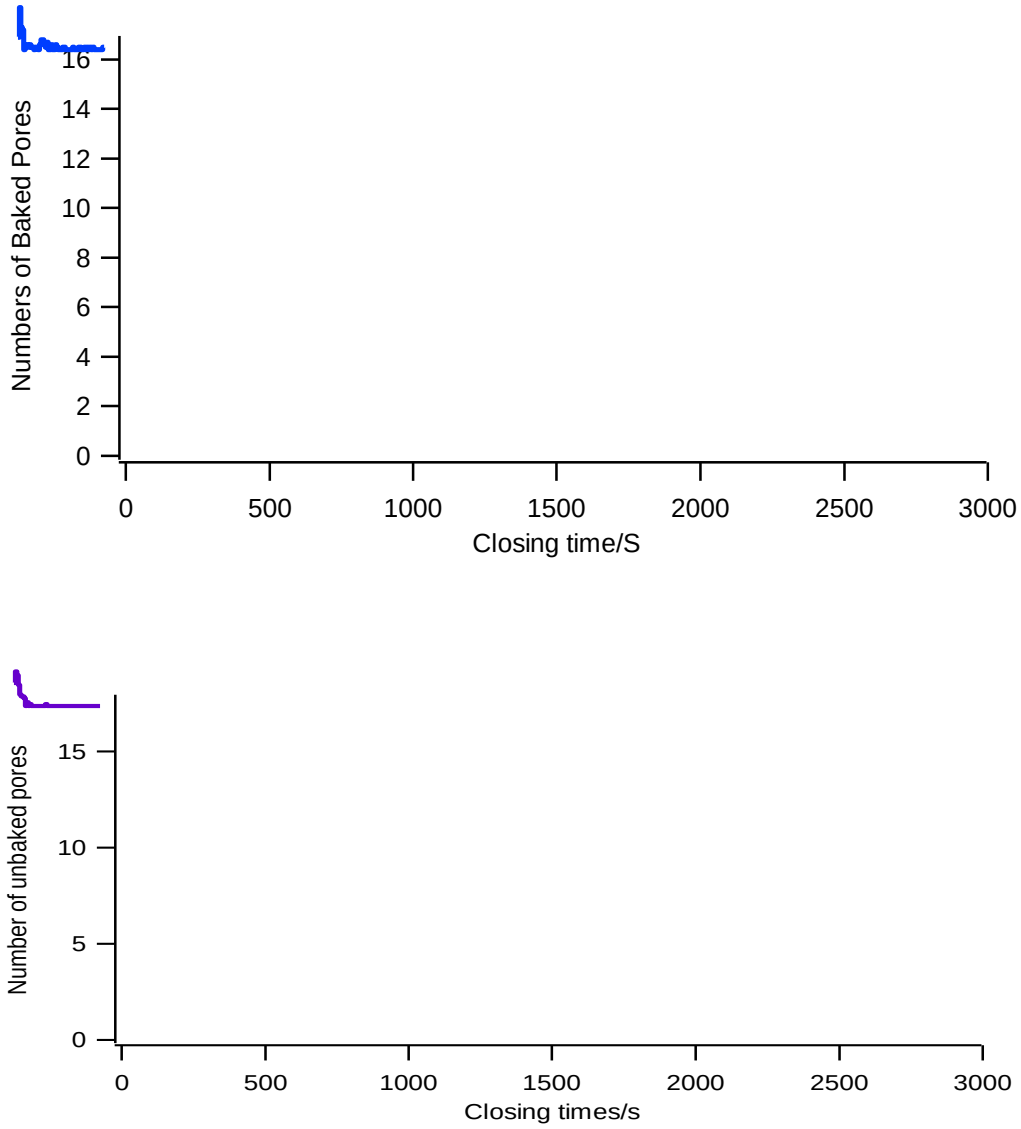

Figure 23: Histogram of baked pores(top) and Unbaked Pores(bottom)

3.9 Surface Adatom Diffusion MODEL

This is one of the fundamental models governing the sculpting of Nanopores. This model assumes that when an incident ion beam or any noble gas ion strikes the silicon nitride surface of a sample in a Fabrication process, some mechanical damage is done resulting in the generation of surface adatoms. The collision of these energetic ions with the surface atoms result in a transfer of energy from the ions to the atoms. Some of these surface atoms may lose energy as a result of

multiple collisions with neighboring atoms and don't make it to the FIB area. The more energetic atoms are ejected from the surface altogether while some atoms have enough energy to travel around the surface as surface adatoms. The surface adatoms are primarily responsible for the closure of pores.

When surface adatoms are created, a concentration gradient is established on the sample surface since the FIB acts as a sink and the rest of the surface around it is populated with atoms. As a result this gradient, surface adatoms will tend to diffuse toward the FIB and will form a thin layer of material around it in a growth pattern resulting in its closure.

The Concentration of Surface Adatoms C(r,t) is governed by the two dimensional diffusion equation

$$\frac{\partial C(r,t)}{\partial t} = \Phi Y_a - \Phi C\sigma - \frac{C}{\tau_{trap}} - D\nabla^2 C$$

Where C(r,t) is the concentration of surface adatoms at time t, r represents the surface position of adatoms from the pore. The first term to the right ΦY_a is the adatom creation term, where Φ is the flux and Ya is the adatom diffusion yield which is the average number of adatoms generated per incident ion. The second term $\Phi C\sigma$ is the annihilation by ion impingement term and represents the probability that the adatom is ejected from the surface. In this term, σ represents the surface area of the adatom. The third term $\frac{C}{\tau_{trap}}$ is the annihilation of adatoms at defects in the material where τ_{trap} is the life time of an adatom. This term would normally represent an adatom that is ejected but trapped for a while due to defects in the material. The last or fourth term $D\nabla^2 C$ is the diffusion term representing the flow of adatoms to the pore boundary

as a result of the concentration gradient. D represents the diffusion coefficient. This term is responsible for the closing of the nanopore.

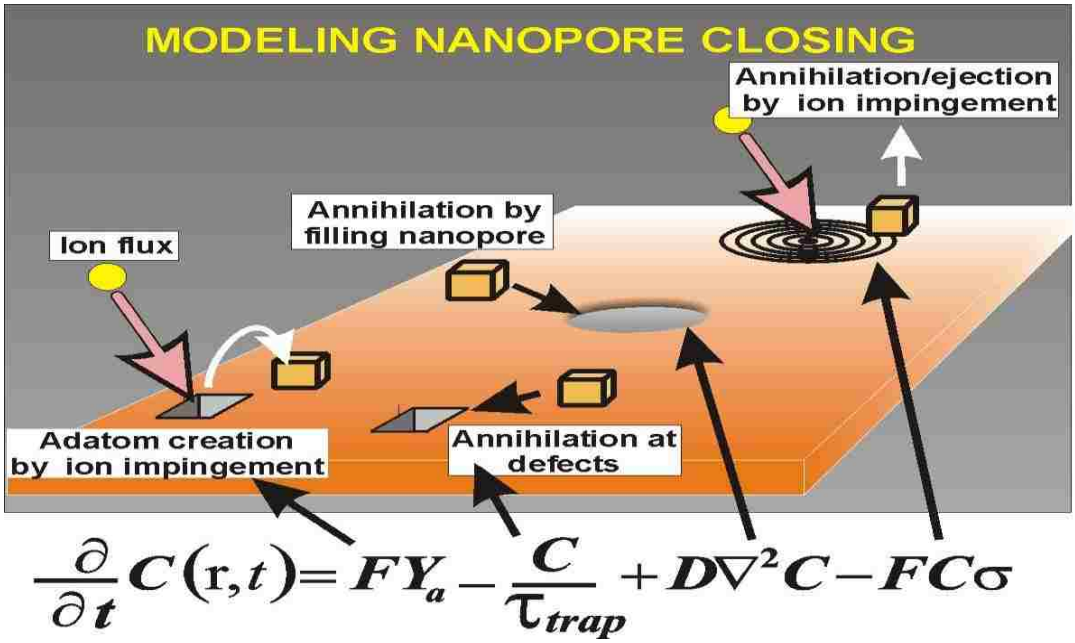

Figure 24: Creation and annihilation process from the adatom diffusion model

Under steady state conditions, $\frac{\partial C}{\partial t} = 0$ and with no angular dependence, $\nabla^2 C = 0$. At $r \to \infty$ the concentration of surface adatoms gives a change in nanopore thickness with respect to area according the equation below

$$\frac{\partial A}{\partial t} = \frac{\partial(\pi R^2)}{\partial t} = -\frac{2\pi\Omega R\Phi}{H}\left(Y_a X_m \frac{K_1}{K_o}\frac{\left(\frac{R}{X_m}\right)}{\left(\frac{R}{X_m}\right)} - Y_p \right)$$

Where Ω represents the adatom cross section, H = pore thickness, R = radius, Y_a is the adatom yield, X_m = diffusion length, Y_p = sputtering term from the nanopore edge, K_1 and K_o are the

modified Bessel function of the second kind. The above equation can be rearranged into two processes that describes the nanopore area changing rate as follows

$$\frac{\partial A}{\partial t} = -\left(\frac{2\pi\Omega R\Phi}{H}\right)\frac{K_1}{K_o}\frac{\left(\frac{R}{X_m}\right)}{\left(\frac{R}{X_m}\right)}Y_a X_m + \left(\frac{2\pi\Omega R\Phi}{H}\right)Y_p$$

This equation shows that the nanopore area changing rate is governed by two processes. The first term to the right represents the closing rate from surface diffusion while the second term represents the opening rate from ion sputtering. The closing rate of the nanopore area is the difference between the closing rate from surface diffusion and the opening rate from Ion sputtering. The surface adatom diffusion model is incorporated into a program called IGOR, which is used to analyze the data from the pore closing process. IGOR uses an algorithm to calculate the time required to close a pore to the radius that was entered at the beginning of the calculation. The area of the pore is then graphed versus the time from the modeling algorithm.

Pore closing and opening rate is also highly dependent on temperature as has been shown from experiments using the sculpting system. At room temperature only the closing term dominates and a pore will close as shown in the figure below

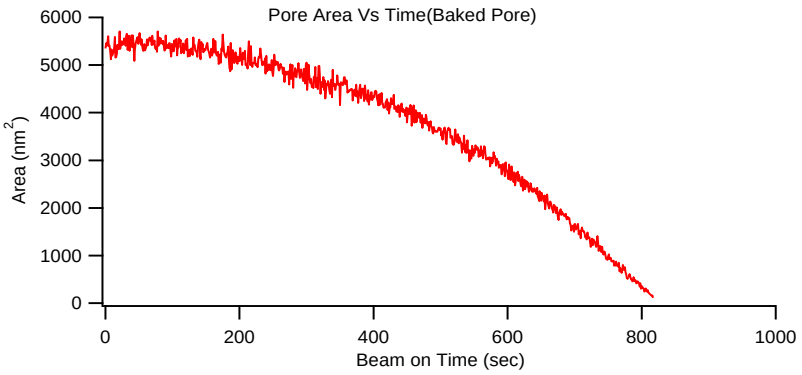

Figure 25: Pore closing slowly at room temperature

The above closing profile is a concave shaped graph in which the area of the pore slowly increases before reaching and inflexion point and then decreases linearly. A plausible explanation could be the removal or cleaning of some material from the edges of the FIB at the beginning of the sculpting process, yielding an increase in the number of counts detected. After this material is removed, the pore closes normally.

The Sculpting chamber can also be cooled to below room temperature by flowing liquid nitrogen through the copper cooling tube until the temperature of the sample is below the desired closing temperature. Previous research indicates that the temperature at which the two processes are equally important is in the range of $0\text{-}10^0$C, under the proper conditions. The pore can be made to close or open when it is above or below this temperature range under the same flux conditions. This suggests that Ion beam sputtering dominates at temperatures below zero while adatom diffusion and pore closure dominates above 10^0C. Ion beam sculpting at low temperatures has been used to open already closed pores by bombarding them with neon ions at 3keV until some counts are recorded on the channeltron.

Pores have also been shown to thin down when they are bombarded with neon ions at low temperatures of about -100^0C. In order to thin down a pore to a specific thickness, the sputtering yield must be known. The formula that relates the sputtering yield and Nanopore thickness is as shown below

$H = F.t.Y_s 0.01 nm^3/atom$

Where H= thickness, F = flux, t = sputtering time and Y_s is the sputtering yield. The sputtering yield is the number of atoms removed per ions hitting the surface of the membrane. Y_s can be determined theoretically from the TRIM program. If the sputtering yield Y_s, the time t and the

Flux F are known, the thickness H of the sculpted pore can be predicted. The setup window for this program and how it works is shown in figure 26.

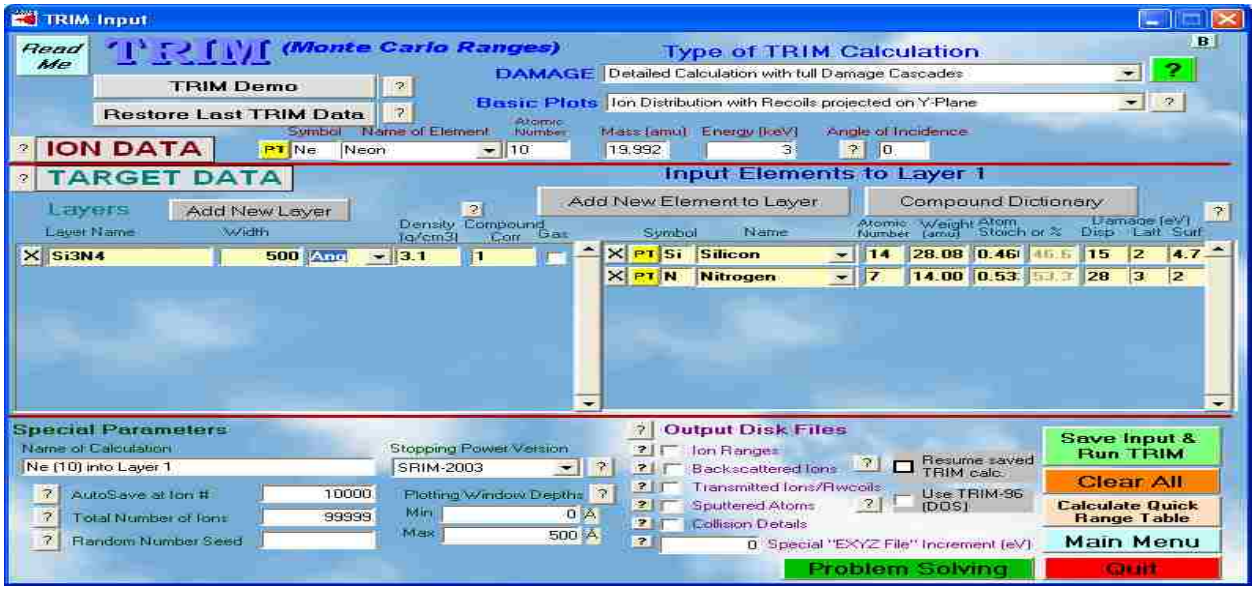

Figure 26: TRIM Setup window

The specific ion required for sputtering can be selected from the list of elements in the periodic table PT menu. Neon ion of energy 3kev is selected from the Ion Data since it is the Ion and energy used in our fabrication experiments. The Target layer is Si_3N_4 and this is selected by adding the new layer tab. The type of TRIM calculation can be chosen by selecting Detailed Calculation with full Damage Cascades. The program has the option of displaying the sputtering process in a variety of plots and the basic plot of choice for the run is the Ion Distribution with Recoils projected on the Y-Plane. Once every parameter has been set up as shown in figure 26, the program is run by clicking on the Save Input and run TRIM. As the program runs, a detailed analysis of the ion motion inside of the target material can be monitored on the XY longitudinal plot as shown in figure 27. The program displays the theoretical value of the sputtering yield for Neon and these values would continue to change until the ions hit their desired target distance

within the silicon Nitride membrane.

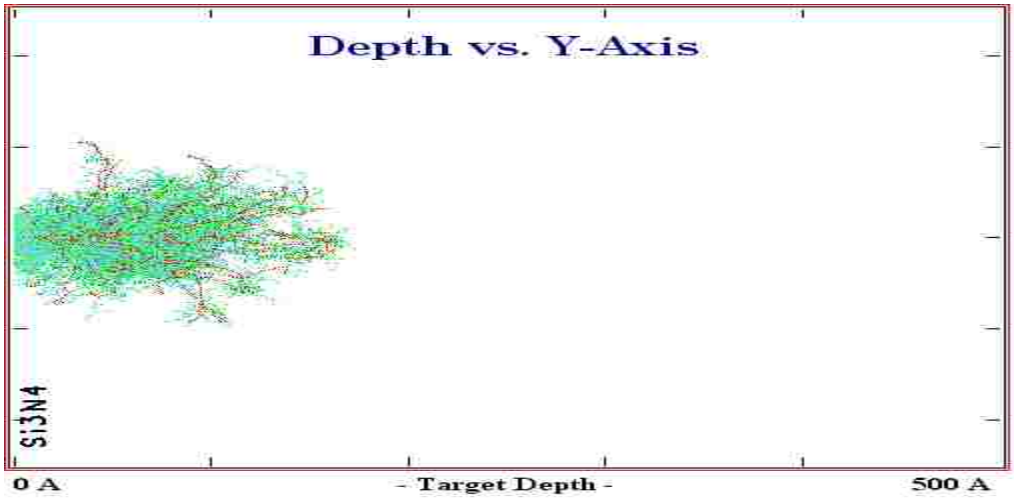

Figure 27: The full damage of ions in Silicon Nitride and the Ion penetration depth

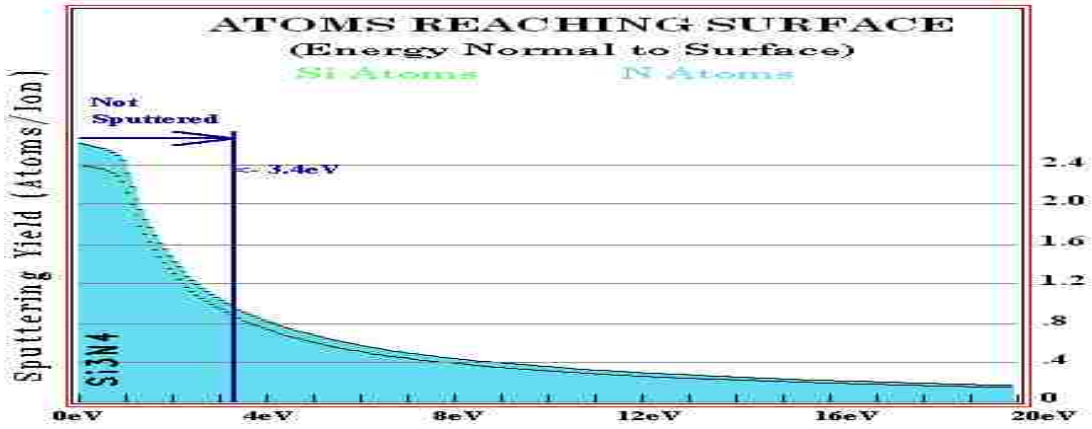

Figure 28: Sputtering Yield Vs Energy

A curve of sputtering Yield versus Energy is plotted as shown in figure 28. This curve shows that only sputtered surface adatoms of Si_3N_4 of energy greater than 3.4ev leave the surface while those not sputtered remain on the surface.

The Sputtering yield for Si_3N_4 can be calculated at the end of the program by adding the individual sputter yields for nitrogen and Silicon. This gives a value of 2.1 atoms/ion for Si_3N_4 when the right energy parameters are applied in the program. Factors that affect the sputter yield are the surface roughness of the material, compound stochiometry and the surface binding energy

which you input into the calculation. The sputter yield determined from TRIM was used to estimate the thickness of a pore after it was sputtered in the Ion Beam sculpting system. A closed pore AR#07201001 was sputtered open by bombarding it with 3kev Ne ions at -100^0C. The pore opening was monitored by using the lab view program. The thickness of the pore was determined from $H = F.t.Y_s 0.01 nm^3/atom$, where the flux F is calculated by dividing the last number of counts when the nanopore opened by the measured area of the opened nanopore. Since the number of counts fluctuates, last number of counts may not accurately represent the final size needed for the flux calculation used for determining the nanopore thickness. Taking an average of the last 5 data points, should give a better representation of the final counts. However, fluxes calculated with the average number of counts are not significantly different from fluxes calculated with just the final count. A graph of counts versus time is shown in figure 29.

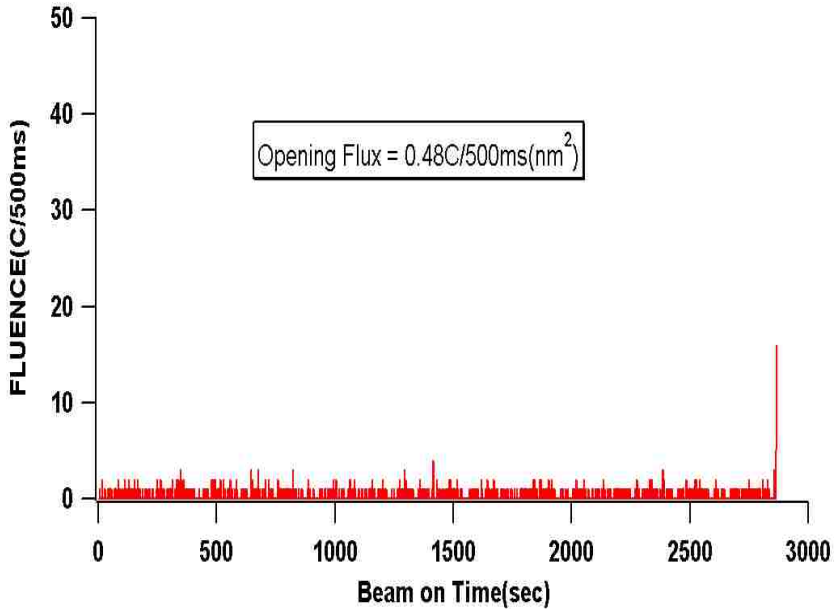

Figure 29: Pore opening by sputtering at -100^oC

As can be seen from the graph, the counter initially records zero counts until after about 2800s when the counts suddenly increased indicating an opening of the pore. Given the time t, the Flux F and the sputter yield as obtained from TRIM, the thickness of the pore can now be calculated.

By plugging in the values for F, t and Ys, it was shown that the pore thickness H = (0.48 ions/0.5s (nm^2)) X (2800s) X (2.1atoms/ions)X0.01nm^3/atoms = 56.4nm. This value is less than the EELS thickness value of 58nm before the sputtering was applied to the sample. This shows that when pores are sputtered at low temperatures, there is an opening and a thinning effect on the pore.

4. Transmission Electron Microscopy

Transmission Electron Microscopes are very powerful and versatile tools used for the characterization of materials. TEMs were developed because of the limited image resolution in light microscopes which is imposed by the wavelength of visible light. This technique transmits a beam of high energy electrons through an ultra thin specimen, interacting with the specimen as it passes through. An image is formed from the interaction of the electrons transmitted through the specimen; the image is magnified and focused onto an imaging device, such as a fluorescent screen.

4.1 Basic Operating Principle

The "Virtual Source" at the top of a TEM represents the electron gun, producing a stream of monochromatic electrons. As the electrons move down the microscope column, its path can be controlled by means magnetic and electrostatic lenses such as the condenser, objective and the projector lenses. The condenser lenses controls the spot size while the objective lenses focus the transmitted beam through the specimen into an image. The image strikes the phosphor image screen and light is generated, allowing the user to see the image. These lenses also have the capability of controlling the intensity, magnification, astigmatism and energy dispersion of the image. The most common mode of operation for a TEM is the bright field imaging mode. In this mode the contrast formation, when considered classically, is formed directly by occlusion and absorption of electrons in the sample. Thicker regions of the sample or regions with a higher atomic number will appear dark, while regions with no sample in the beam path will appear bright hence the term "bright field".

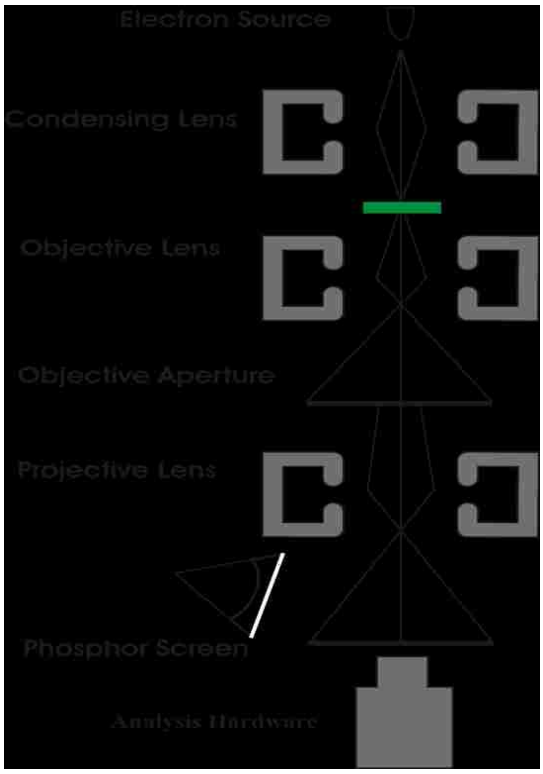

Figure 30: Electron path as it travels down a TEM Column

4.2 TEM Resolution

TEM resolution is the ability of the microscope to make points, which are closely adjacent in the object, distinguishable in the image. TEM resolution is then defined to mean the "minimum resolvable distance" in the object. The image resolution in the TEM is governed by the ability of the objective lens to image the object. The resolution can be limited by Chromatic aberration, Spherical aberration and astigmatism. Spherical aberration is caused by the lens field acting in homogeneously on the off axis rays. Chromatic aberration results in electrons with a range of energies being focused in different planes. Electrons emerging from the specimen with no loss of energy are less strongly focused by the objective lens than those that suffered energy loss in the specimen, so a point is imaged as a disk. Astigmatism occurs when the electrons sense a non-uniform magnetic field as they spiral round the optic axis. Astigmatism can be corrected by using

stigmators, which are small octopules that introduce a compensating field to balance the inhomogeneities causing the astigmatism

By changing the parameters of the lenses, the user is changing the angles in which the beam above and below is collected .Figure 31 gives a diagrammatic description of the beam collection process. α is the image collection half-angle and β is the object collection half-angle. The object collection angle is the most important for it determines the range of energies that are collected as spectra for analysis.

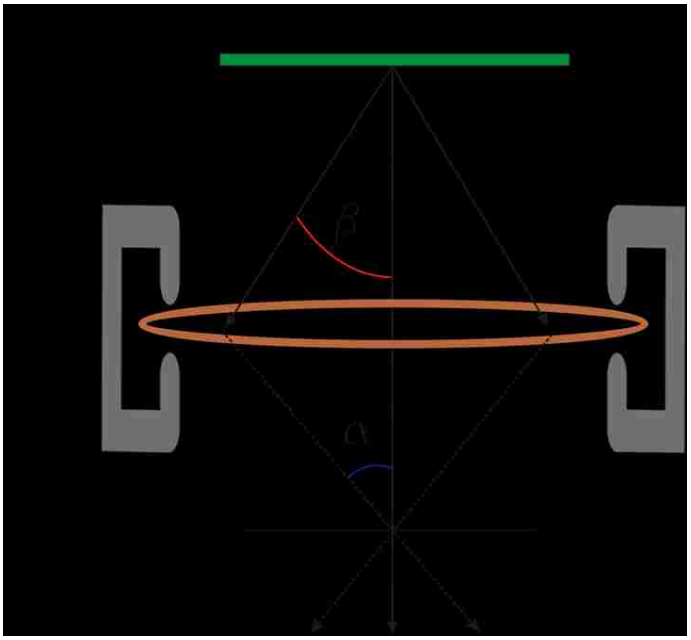

Figure 31: Object and Image collection half angles

When the apertures are inserted, usually after the condenser, objective, or projective lenses, they limit β by blocking highly scattered electrons and can increase the resolution of the image.

The main advantage of the Electron microscopy over other imaging techniques is its ability to image at a very high resolution. The relationship between the accelerating voltage and the wavelength of the electrons above 100keV is a relativistic one because the velocity of electrons becomes greater than half the speed of light. The accelerating voltage of the FEI Titan TEM

located at the University of Arkansas has a setting of 300kV. This gives a relativistic wavelength limit of about 2pm according to table 1.2 in Williams and Carter. Since most of the samples used for this project were imaged using the Titan TEM, one can infer that a sub angstrom resolution less than that of the diameter of an atom was attained. TEM has also been used to image various biomolecues and the chart below shows the various resolution limits of the TEM to different biomolecules.

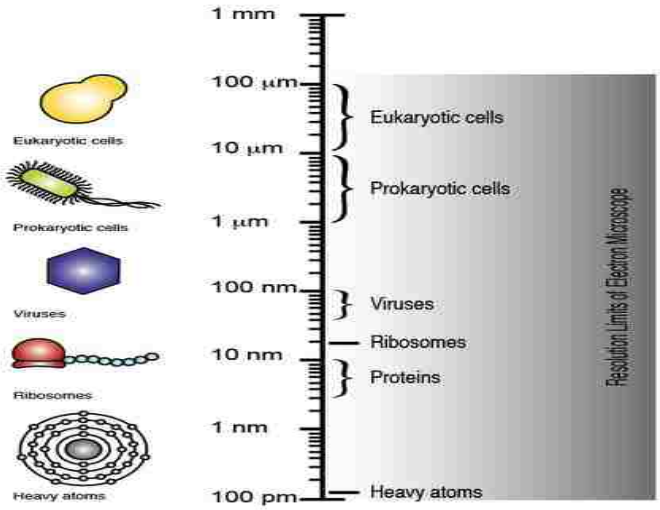

Figure 32: Resolution limits of the TEM

The relationship between the accelerating voltage and the wavelength is given by the equation $\lambda = \frac{h}{\left[2m_0 eV\left(1+\frac{eV}{2m_0 c^2}\right)\right]^{1/2}}$. Where λ is the electron wavelength is, h = Planck constant, V = the accelerating voltage of the electron microscope, m_0 = rest mass and c is the speed of light in vacuum. By increasing the accelerating voltage of the microscope, we decrease the relativistic wavelength of the electrons and hence an increase in the resolution of microscope.

5. Thin Film Thickness Measurement

Thickness measurement and analyses of nanopores fabricated by the ion beam sculpting technique is extremely important since the thickness of a pore determines its resolution capabilities in translocation experiments. The Nanospec is one such equipment used in measuring the thickness of the bulk membrane of silicon nitride samples in the wafer preparation process and also in the thinning of fabricated pores during the RIE process.

5.1 The Nanospec

The NanoSpec at the HiDEC Center is a computerized Film Thickness Measurement System for bulk membranes. It is used for measuring the thickness of optically transparent thin films (10nm-4000nm) on silicon wafers. It is based on the principle that the Intensity of reflected monochromatic light depends strongly on film thickness. Typical Nanospec thicknesses for Si_3N_4 samples used for this research ranged from 2750-3311A^0. The NanoSpec is unable to measure thicknesses less than 100A^0 and would normally display an "Out of Range" result for such thicknesses. The NanoSpec would also give an "Out of Range thickness" measurement if the sample is dirty and if it can't recognize the thin film type under study. The film thicknesses are comparable to the wavelength of light. The equipment is composed of a spectrophotometer head, photo-intensity display, wavelength dial, fine and course focus and a reference silicon wafer.

Figure 33: Overview of the NanoSpec

The Spectrophotometer head mounts unto a customized microscope with vertical reflected light using a regulated tungsten lamp, variable field diaphragm, 10X, 100X and 40X objectives. The Spectrophotometer head has a diffraction grating monochromator that rotates. Reflected light coming from the sample, passes through the slit to the collimator and then to the grating. As the grating rotates, it shines different frequencies of light unto the detector. Each wavelength of light is focused to a different position at the detector, and the wavelength which is transmitted depends on the rotation angle of the grating. The lights reaching the detector interfere with one another to form a sinusoidal pattern of intensity Vs wavelength. A curve-matching algorithm is used in the computer to yield rapid and precise thickness readings. This algorithm will try to match the sinusoidal pattern from the sample to that of the reference wafer. Given the index of refraction for a thin film and the two measured spectrums, the computer will analyze the interference pattern to determine the film thickness.

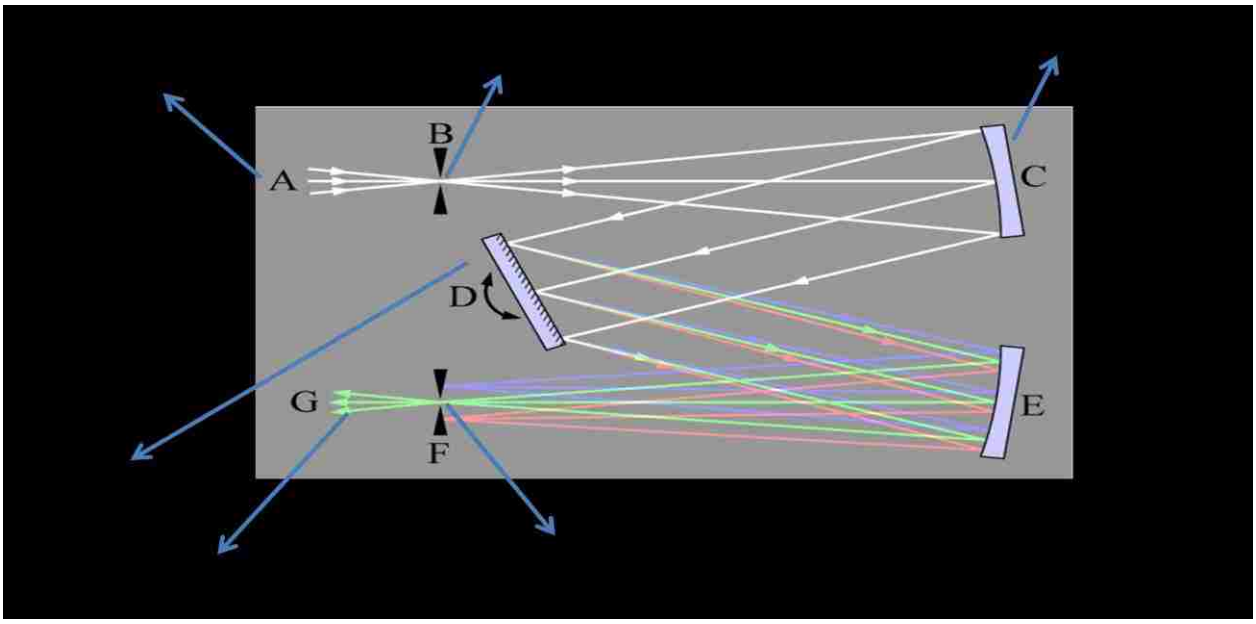

Figure 34: The Spectrophotometer Head

5.2 Determination of the Etch-Rate of Silicon Nitride

In order to thin nanopores, the etch–rate of the Silicon Nitride used in its fabrication must be determined. The most common technique used in this process is the reactive Ion etching technique already described above. Nanospec measurements were performed at different parts of each silicon nitride sample and the average calculated. Taking measurements at different parts of the sample and averaging the results helps minimize errors. Each of these samples were then etched repeatedly by reactive Ion etching with the results as shown in table 5

Measurement	Pre-Etch Thickness (0S)	Post-Etch Thickness (30s)	Post-Etch Thickness (60s)	Post-Etch Thickness (90s)	Post-Etch Thickness (120s)
1	2457A	2286A	2171A	2065A	1898A
2	2456A	2289A	2167A	2063A	1896A
3	2446A	2286A	2168A	2040A	1905A
4	2453A	2287A	2186A	2036A	1901A
5	2472A	2314A	2190A	2050A	1912A
Average Thickness	2456A	2292.4A	2176.4A	2050.8A	1902.2a
Thickness Removed	0	164.4A	280A	406A	554.6A

Table 5: Nanospec measurements of thickness removed Vs Etch Time.

The amount of thickness of Si_3N_4 removed was determined by first calculating the average of thickness after every RIE Process and subtracting it from the previous thickness measured. A graph of thickness removed Vs Etch-time was then plotted as shown in figure 35

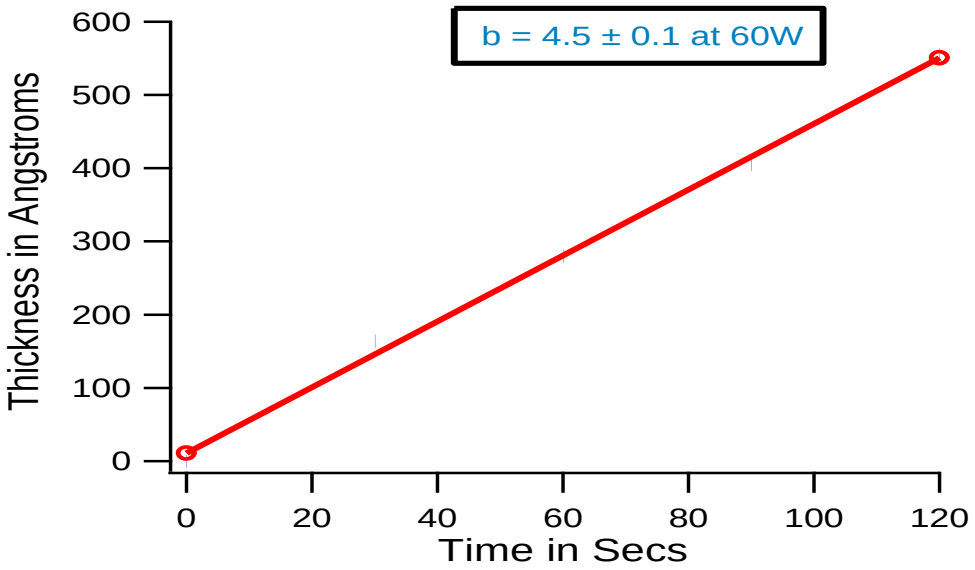

Figure 35: Graph of Thickness of Si_3N_4 removed Vs etch time at 60W RIE Power

The linearity of the above graph is as expected and the etch-rate was found to be 4.5 A^0/S. An image analysis of a TEM image before and after the RIE process is shown in figure36. The post-RIE image looks much brighter than the Pre-RIE Image. The brightness suggests the post RIE is thinner than the pre-RIE image since more light (electrons) can pass through the post RIE without being absorbed. The success of the RIE can be further investigated by doing a thickness map analysis of the pre and post RIE images to ascertain exactly how much material was removed

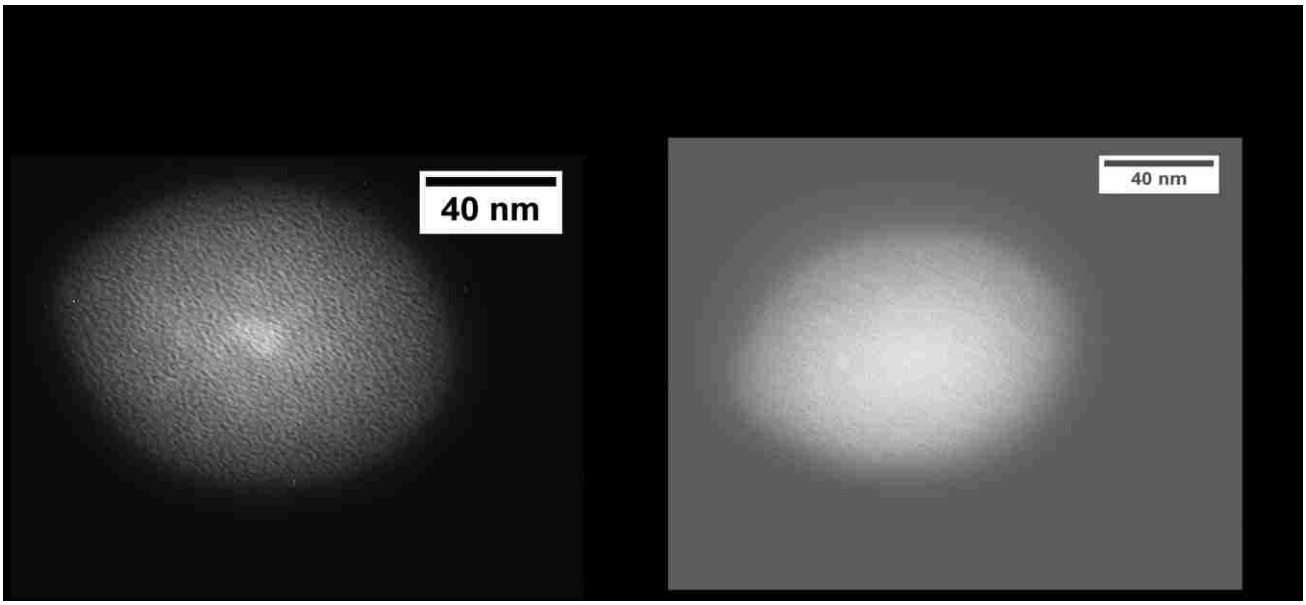

Figure 36: Post and Pre-RIE Images

Figure 37 below shows the thickness map analysis of the images in figure 36.

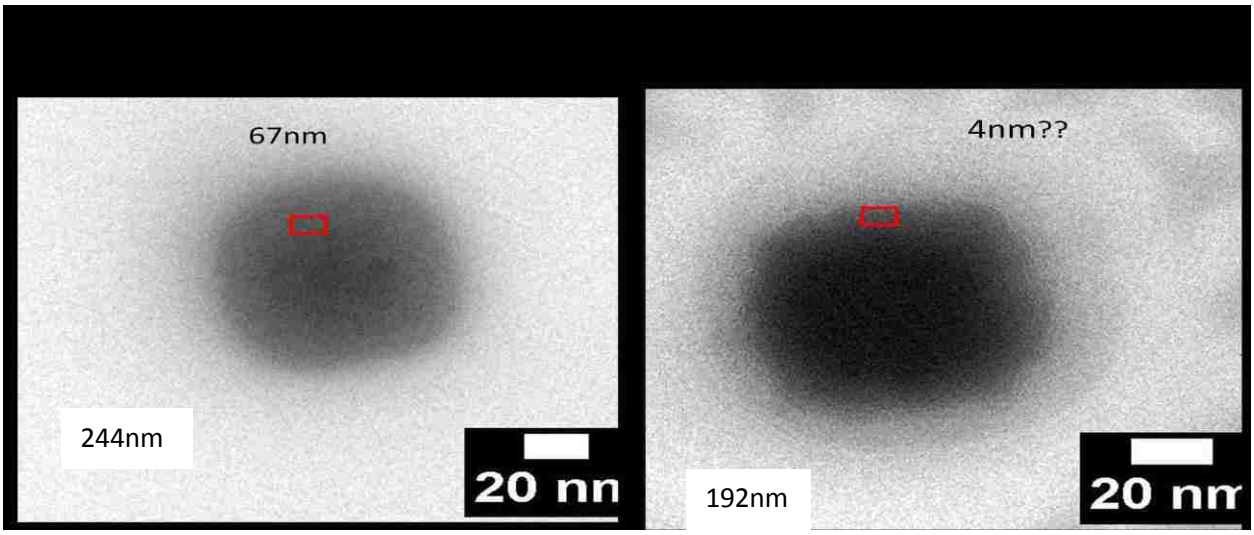

Figure 37: Thickness Map analysis of pre-RIE (Left) and post-RIE (Right)

The above figure shows that the membrane thickness decreased from 244nm to 192 nm implying 52nm of the membrane was etched away. The red rectangle on the figure shows the area were the measurement of pore thickness before and after the RIE was taken. Pore thickness decreased from 67nm to about 4nm indicating that about 63nm of material was etched away. When the

differences in the amount of material etched between the membrane and pore regions are compared we see a difference of about 11nm. This is not much at the Nanoscale and so we conclude that the etching by RIE was indeed successful.

5.3 Nanopore Thinning by Reactive Ion Etching

From the current blockade equation $\Delta I == V\sigma \frac{A_{DNA}}{L_{pore}}$, thinner pores would measure a higher current drop and would help enhance the resolution of DNA molecules when passing through them. The main goal of this project was to thin select samples of Nanopores with pits to a specified thickness by using the reactive Ion Etching technique. Samples with pits are those whose FIBs have been closed all the way in the fabrication process.

Before the RIE Process was performed, a TEM EELS pre-thinning measurement was done by taking pictures at about 160kx magnification. Thickness maps were taken at about 10µm from pore. The TEM imaging also gives us information as to which FIB have pits on them and what the thickness of these pits are. In order to etch the select samples, an etch-rate check was performed by etching various test samples of Si_3N_4. The main reason for running an etch-rate test is to verify consistency with the previously determined etch-rate value of silicon nitride. The system is set running for sometime before beginning the etching process in order to ensure stability. Once the system is stable, the etch-rate values become very consistent and repeatable. Each sample slated for etching is first primed for about 20s before running the actual etching recipe. The priming helps clear the sample of any dirt or impurities. The cleaning is evident since the samples emerge from the RIE looking cleaner than before they were put inside. As can be seen in figure 38, the etching rate dropped to about half its value at 100W when the RIE power was halved to 50W. This is a clear indication that the etching rate is directly proportional to the RIE power. The Idea of using a smaller etch-rate is to be able to have a greater control over the

amount of material removed from the sample. The etching process was carried out by etching the samples, taking Nanospec measurements and computing the etch-rate at different times. The average etch-rate for a 50W power setting of the RIE was about (10±2)nm/min for the samples examined and was highly repeatable.

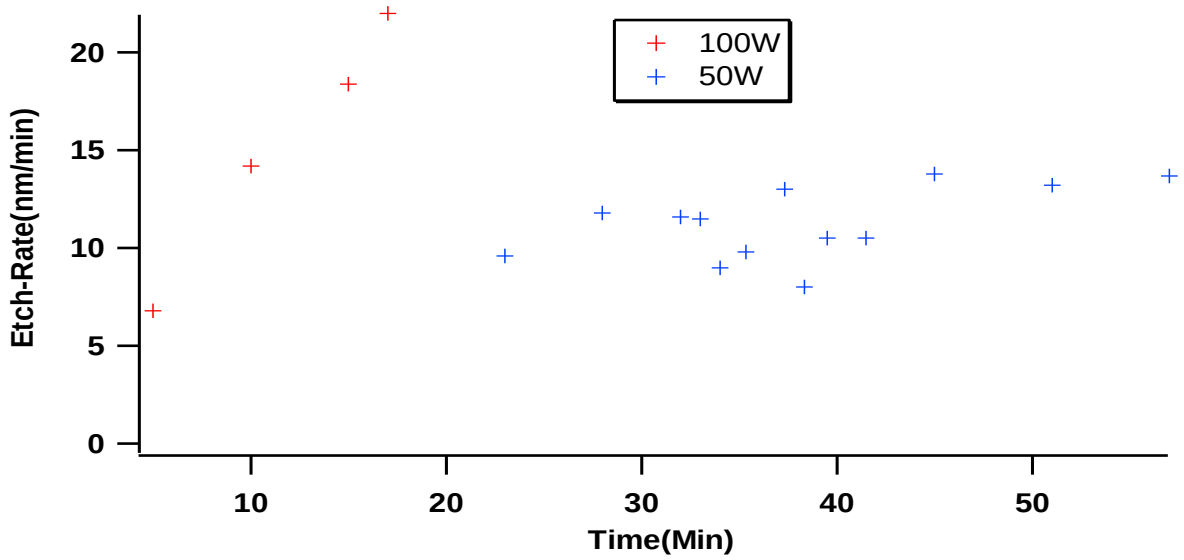

Figure 38: Etch-rate test Data for samples separately etched at different instances of time

The red points on the graph shows etch-rate calculations at 100W power rating of the RIE while the blue show etch-rate calculations at 50W power. The blue dots show a deviation of about ± 4% in the etch-rate data. With this information, four selected samples with pits on them were then etched and the results shown in table 6.

Pore name	Etching time in seconds	EELS pre etch thickness of pit (nm)	Post Etch desired thickness of pit	EELS Post-etch thickness of pit	Change in thickness of pit	Percent Deviation
09-03-11-036	126	81	60	75.6	9.4	20.63
09-03-11-080	198	43	10	16.6	26.6	39.76
09-03-11-060	282	92	45	44.6	47.4	-0.90
09-03-11-072	360	32	Blast open	21.9	10.1	X
09-03-11-092	360	30	Blast open	22.4	7.6	X

Table6

As can be seen from the above table, sample 09-03-11-060 gave the smallest percent deviation of 0.89% while sample 09-03-11-080 gave the highest percent deviation of 39%. The reason for high deviation for sample 09-03-11-080 could be due to dirt or some other impurities within the edges the pore. TEM pictures of the samples before and after the RIE process were analyzed in order to ascertain the impact of the RIE on the pores. The results of this analysis are shown in figure 39.

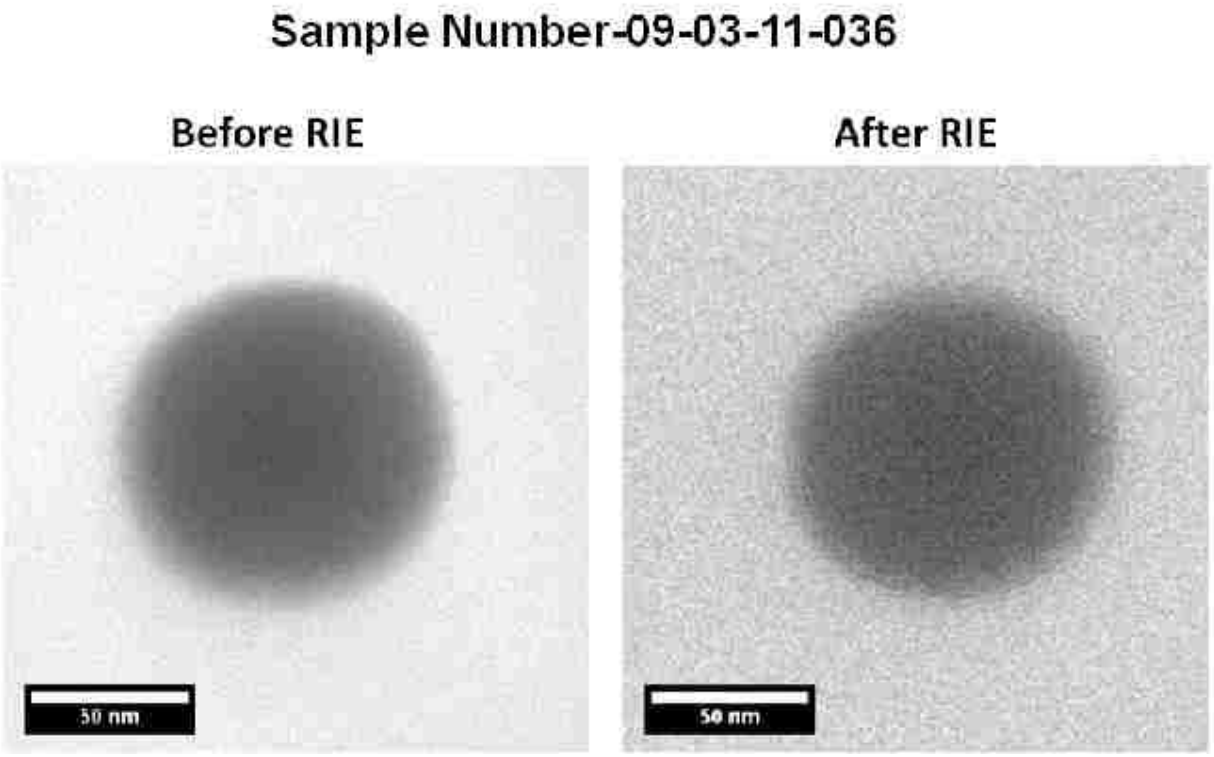

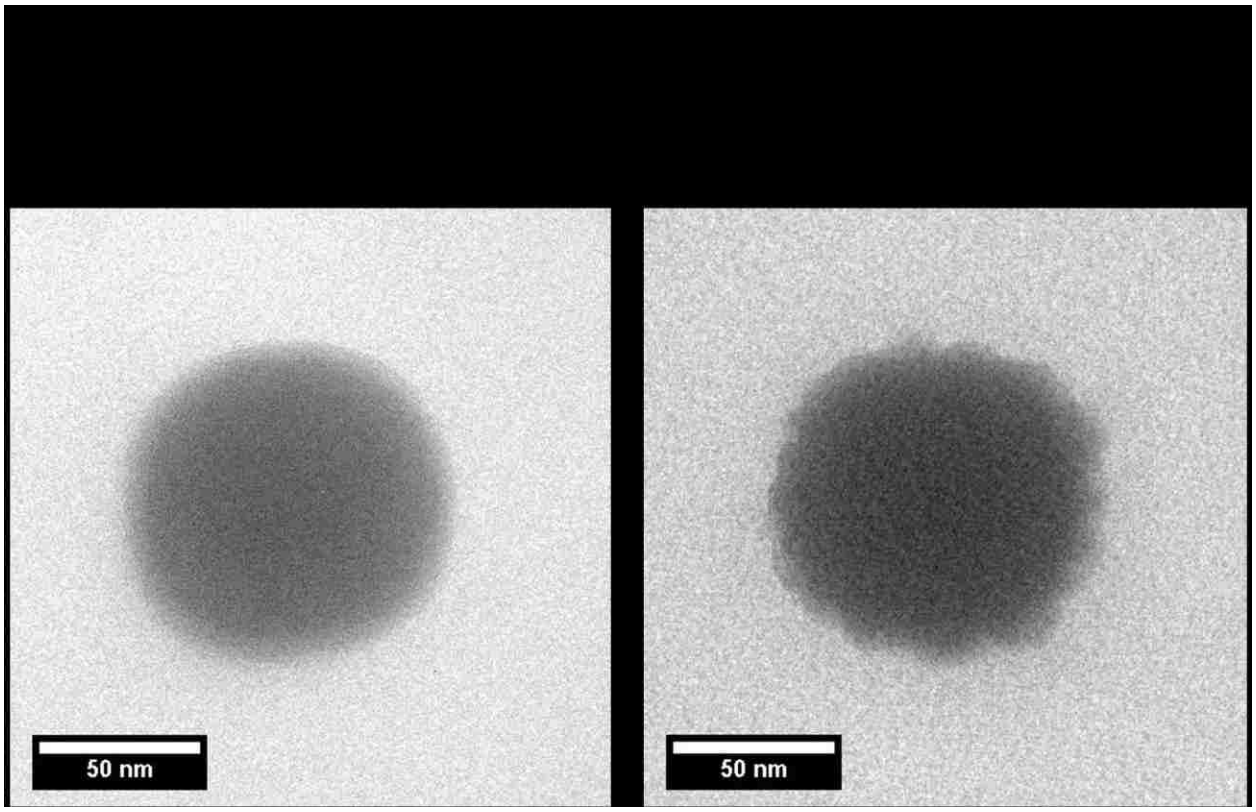

Sample Number 09-03-11-072

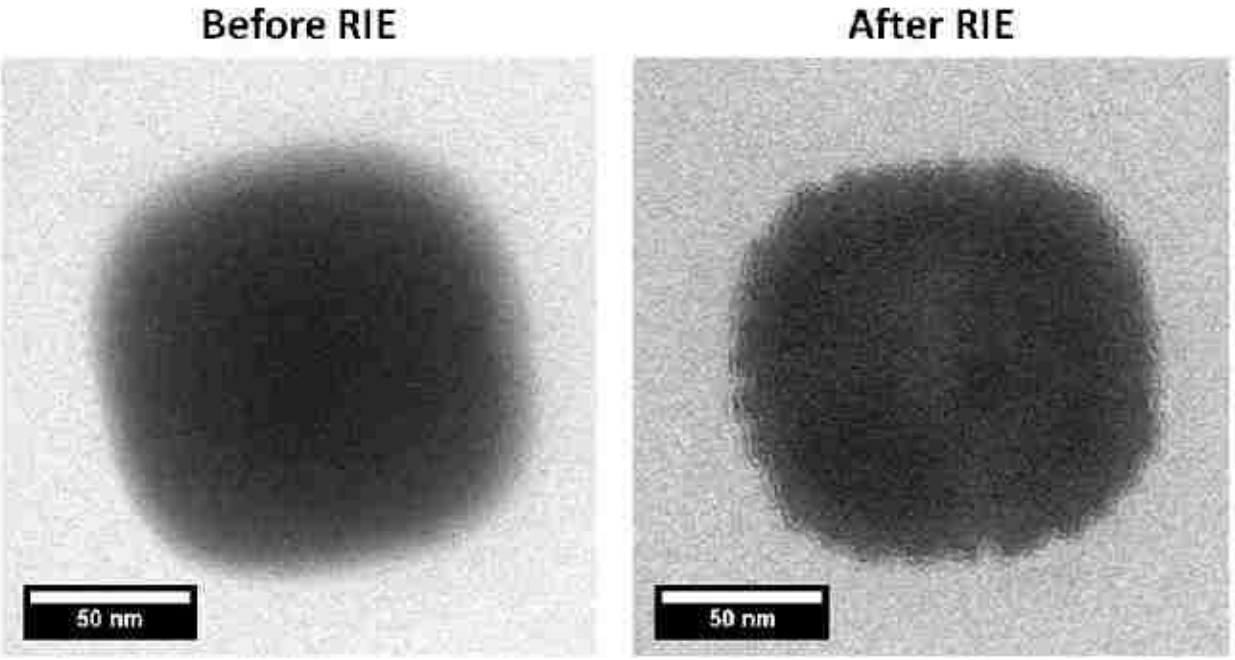

Sample Number - 09-03-11-080

Before RIE

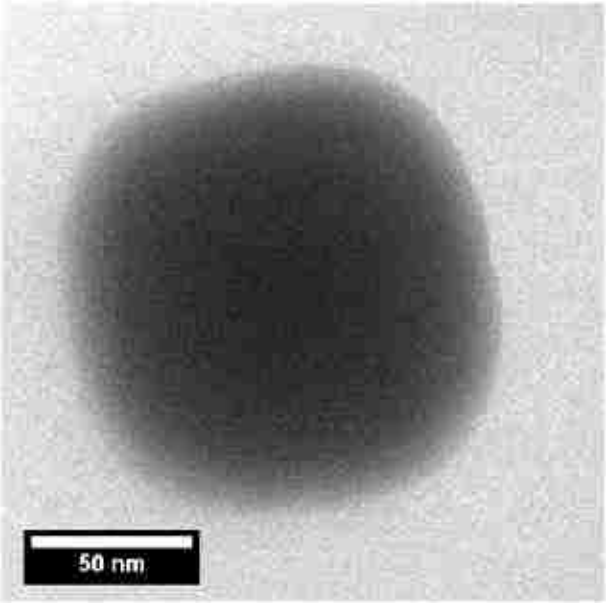

After RIE

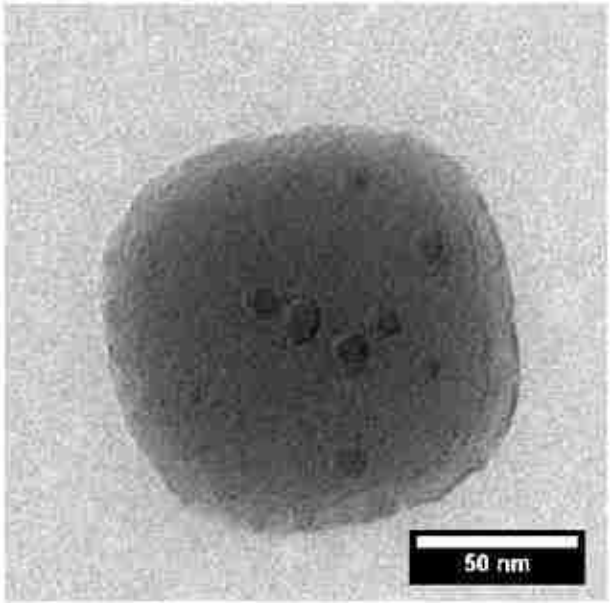

Sample Number - 09-03-11-090

Before RIE

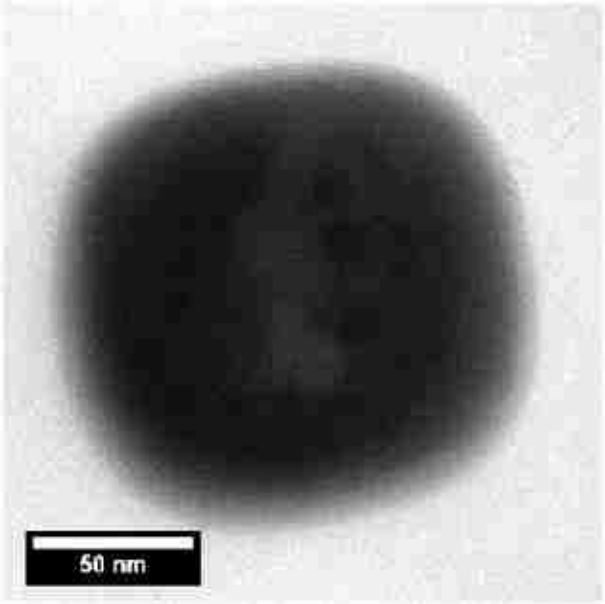

After RIE

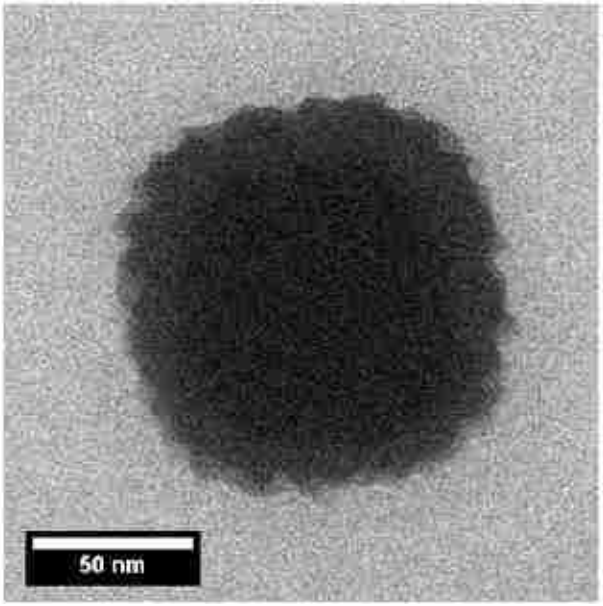

Figure 39: TEM Images of pore before and after RIE

As can be seen from the above pictures, the post RIE TEM pictures have some ripples at the edges leading to the conclusion that an etching effect has indeed taken place.

5.4 The Nanopore Geometric Analysis

A TEM Nanopore thickness map Image of a sculpted pore can be analyzed based on the simple geometric model comprising of the FIB, a nanopore and a cone-like part of the geometry connecting the nanopore and the FIB. Information such as the FIB diameter, pore diameter, FIB thickness, Pore thickness and the cone can be obtained using the EFTEM mode of the TEM, ImageJ and Igor programs. The following procedure outlined below gives a step by step guide as to how these measurements can be carried out. When the thickness map image from the TEM is opened in ImageJ, the thickness the pore can be calculated by:

1) Using ImageJ, draw a rectangle on region of interest on the thickness map.

2) Hit Ctrl-M to measure the relative thickness of the selected region.

3) Multiply the relative thickness by 185nm to get the thickness. 185nm is the scale factor (Mean free path). The mean free path was calculated by taking a 30µm by 30µm window without an FIB hole and measuring the thickness.

4) Repeat steps 1 to 3 two more times on other parts of the membrane and take the average of the results to get the thickness.

The diameter of the pore or FIB can be calculated by using the free hand /line tool

Figure 40: Image J Tool bar

The FIB or pore diameter is determined by drawing a line across the desired diameter using the line tool shown in figure 40. Since the FIB or pore image is often elliptical, the actual diameter of the FIB or Pore is computed by taking the geometric mean of the diameter values across both axes.

The cone angle can be calculated from the thickness map profile from ImageJ and Igor. The profile is found from Image J by using the rectangle tool to draw across the thickness map as shown in figure41 and hitting ctrl+k to obtain the profile data.

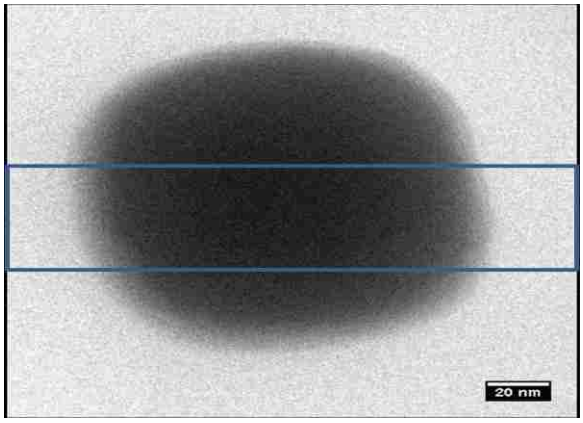

.

Figure 41: Scan of Thickness map using imageJ

This profile data obtained from ImageJ is then imported into Igor and used to plot a graph of relative thickness versus distance as shown below.

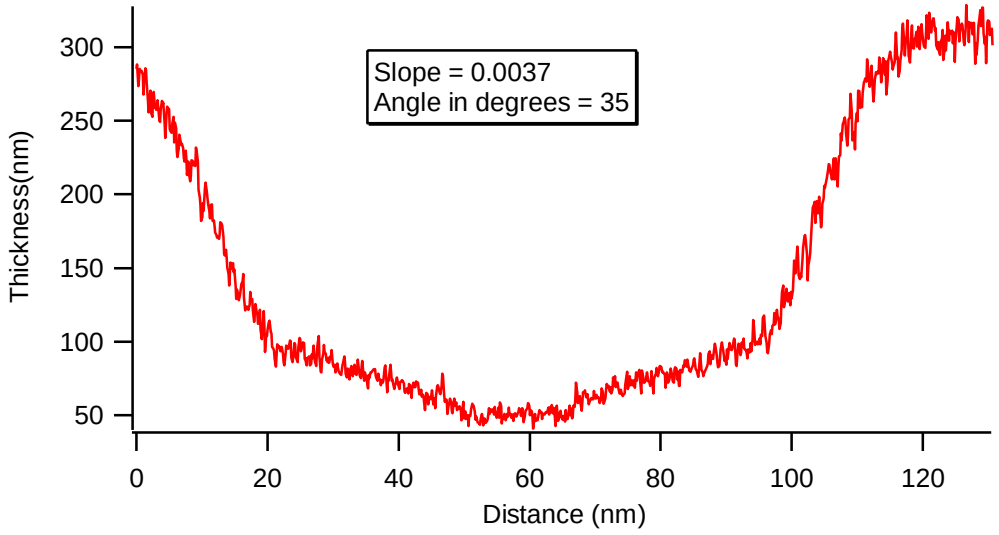

Figure 42: Thickness Vs distance profile for the thickness map as plotted from Igor

The relative thickness = actual thickness/mean free path. The mean free path is obtained from the TEM log ratio calibrations. The slope of the line from the center of the profile corresponding to the cone part of the model and is obtained by selecting that part of the profile and doing a linear fit to get the slope.

The arctangent of the slope then gives the angle of the cone. The height of the cone can then be determined from trigonometry since the angle is known. The thickness of the actual nanopore can be obtained with some accuracy by subtracting the membrane thickness from the sum of the FIB and cone thicknesses.

6. Conclusion

Nanopores have been successfully sculpted by using the Ion Beam sculpting system at the University of Arkansas. Pore closure rate can be controlled by baking them under vacuum conditions up to a temperature of 122^0C for about 10 minutes. A temperature of 122^0C is not sufficient enough to break the bonds between the atoms in a silicon nitride membrane. This can be validated by the fact that TEM Images of pores taken before and after the baking process does not change leading one to suggest other factors must have been responsible for the decrease in pore closing rate after they are baked. When the time between baking a sample in the load-lock under vacuum conditions and closing is small, the closing rate is faster. If the sample is allowed to cool for a longer amount time before the closure, the closure rate is slower. The reason for this change is not well understood at the moment but can be attributed to the growth of an oxide layer on the sample when it is left to cool for a longer time before it is closed. Another reason could possibly be dirt or some other impurities on the surface of the membrane A residual gas analysis of the main chamber for system contamination showed higher composition of water in the chamber when pores closed too fast as opposed to when there was no water. This seems to suggest that water or a moist environment affects pore closure rate. It has also been shown that pores tend to open up when they are cooled to very low temperatures of about -100^0C and therefore suggests that temperature plays a key role in the opening and closing of nanopores.

There has also been the successful thinning of nanopores using the reactive ion etching technique at the High Density electronic Center (HiDEC). Open pore currents for thinned pores are greater than those for thick pores since there is an inverse relation between the current and thickness from the current blockade equation. The thinner the pore, the greater the blockade current would

be in a translocation experiment and the greater the spacial resolution of DNAs passing through the pore.

References

1. *Nanopore sculpting with noble gas ions.* **Cai, Q., et al.** 2006, J. App. Phys., pp. 100, 024914: 1-6.

2. .*Ion-beam sculpting at nanometre length scales.* **Li, J., et al.** 2001, Nature, pp. Jul. Vol. 412: 166-169.

3. *Fabrication of Solid State Nanopores Using Feedback Controlled Ion Beam Sculpting Techniques master's thesis.* **Ledden, B.** 2004.

4. Transmission electron Microscopy basics. David B. Williams and C Barry Carter

5. Control of Shape and Material Composition of Solid-State Nanopores. ***Wu, M.,*** *et al Nano Lett.,* Vol. 9, No. 1, **20**

6. Storm, A. J., Chen, J. H., Ling, X. S., Zandbergen, H. W. & Dekker, C. Fabrication of solid-state nanopores with single-nanometre precision. Nature Materials 2, 537-540 (2003).

7. The effect of ion beam sculpted nanopore size and shape on DNA translocation. Poster presentation. Ryan Rollings APS 2011